Air-entraining admixtures as a protection mechanism for bacterial spores in self-healing cementitious composites: Healing evaluation of early and later-age cracks

Ismael Justo-Reinoso [a,*], Bianca J. Reeksting [b], Charlotte Hamley-Bennett [b], Andrew Heath [a], Susanne Gebhard [b], and Kevin Paine [a]

[a] *University of Bath, Centre for Innovative Construction Materials, Claverton Down, BA2 7AY, Bath, UK*
[b] *University of Bath, Department of Biology & Biochemistry, Milner Centre for Evolution, Claverton Down, BA2 7AY, Bath, UK*

ABSTRACT

Costs associated with the encapsulation process of bacterial spores continue to be a limiting factor for the commercialisation of self-healing cementitious materials. The feasibility of using air-entraining admixtures (AEAs) as an economical and straightforward encapsulation method for bacterial spores was evaluated to heal cracks (~0.50 mm) that were formed at an early (28 days) or later age (9 months). The results showed that not all the AEAs commonly used in concrete industry, can provide sufficient protection to enable the direct addition of bacterial spores when compared to other successfully proven protection methods (i.e., *via* aerated concrete granules (ACGs)). In this regard, only one of the three AEAs investigated improved the healing performance when compared to an equivalent mix using bacterial spores encapsulated in ACGs. Healing ratios obtained with this successful AEA were 59.6% and 46.2% higher than the results observed for the ACGs-containing mix when the cracking age was 28 days and 9 months, respectively. Moreover, water penetration resistance was increased by 18.1% or presented very similar values (~84%) after 56 days of healing for early or later-formed cracks, respectively. Moreover, a simple cost analysis was conducted to confirm the significant economic benefits of using AEAs to protect directly added bacterial spores. In this regard, the cost of using AEAs is about 13 times lower than for ACGs. Therefore, this study provides for the first time, evidence of the feasibility of using AEAs to protect bacterial spores, opening the doors to the development of bespoke AEAs to design cost-efficient self-healing cementitious materials.

Keywords: Air-entraining admixtures; Bacteria; Encapsulation; Later-formed cracks; MICP; Self-healing.

Abbreviations:

ACG	Aerated concrete granule
AEA	Air-entraining admixture
BBSHC	Bacteria-based self-healing concrete
EDX	Energy dispersive X-ray
GM	Growth media
HR	Healing ratio
LB	Lysogeny broth
MICP	Microbially induced carbonate precipitation
SEM	Scanning electron microscope
SH	Self-healing

1. Introduction

Concrete is the most used building material on the planet, but due to its relatively low tensile strength, the appearance of cracks is inevitable and represent one of its inherent weaknesses [1-3]. Small cracks (<0.8 mm in width) may not cause a concrete structure to collapse but are responsible for accelerating its degradation due to the penetration of aggressive agents that rapidly reach reinforcement steel, causing it to corrode [4]. In the last 15 years, intense research on the development of self-healing (SH) cementitious materials capable of closing these small cracks has been performed [5-8]. Different SH strategies have been investigated, focusing

* Corresponding author
E-mail addresses: ijr27@bath.ac.uk (I. Justo-Reinoso), b.j.reeksting@bath.ac.uk (B.J. Reeksting), pr1cemb@bath.ac.uk (Ch. Hamley-Bennett), a.heath@bath.ac.uk (A. Heath), s.gebhard@bath.ac.uk (S. Gebhard), k.paine@bath.ac.uk (K. Paine).

principally on the use of microcapsules containing mineral healing agents [9-11] and microbially induced carbonate precipitation (MICP) [5, 7, 12, 13].

In MICP, calcium carbonates ($CaCO_3$) are precipitated as a side effect of the biological activity of alkaliphilic bacteria able to tolerate and thrive under the environmental conditions present in the concrete surface [14, 15]. Thus, MICP represents a promising strategy to achieve sustainable bacteria-based self-healing concretes (BBSHCs). For BBSHCs, spores are preferably used, rather than vegetative cells, for their ability to remain dormant for years and activate once water and oxygen ingress through the newly formed crack. However, to be viable when these cracks occur, spores must be protected from the initial harsh conditions present during the mixing and hardening phases. Consequently, different encapsulation strategies have been developed to guarantee enough viable spores will be present once the cracks are formed. These encapsulation strategies consist of immobilising the bacterial spores within a protective carrier, commonly using porous particles [16-19], polymer-based capsules [20, 21], powder-compressed particles [22] and hydrogels [23, 24]. However, despite the advances made in recent years, the encapsulation process continues to be expensive, with estimated costs between €30 and €50/kg of bacterial spores depending on the encapsulation process used [25]. Consequently, the cost of encapsulated bacterial spores continues to be a limiting factor for the commercialisation of BBSHCs and there is an urgent need to reduce the costs associated with the encapsulation of bacterial spores.

In this regard, a very promising alternative is the use of air-entraining admixtures (AEAs) as the protection mechanism. AEA incorporate tiny micro-bubbles throughout the concrete matrix during the mixing process. These air voids promote the durability of concrete during freeze-thaw cycles and improve its workability [26-28]. AEAs comprises a group of surfactants characterised by possessing a hydrophobic tail and a charged hydrophilic head [29], where the charge of the latter classifies them into: amphoteric, cationic, anionic and nonionic [30, 31]. Anionic surfactants, such as sulfonated hydrocarbon-soluble salts, lignin sulfonate and sodium oleate, are the most commonly used in the concrete industry [31-33]. Nonionic types are less commonly used, while only a few records have been reported for cationic types. [31]. Regardless of the type, micro-bubbles are formed during the mixing process, where the hydrophilic heads of the surfactant counteract the tendency for the dispersed bubbles to coalesce [34] producing a large number of uniformly distributed micro-bubbles with diameters ranging from 0.02 to 1.0 mm [33]. These air voids may enable spores to survive the initial conditions due to an increase in available space and, at the same time, advantageously isolating them from directly mixed nutrients [29]. Moreover, the homogenous distribution of these air voids through the cement matrix will increase the probability of a crack hitting them.

However, even though the main effects related to the use of AEAs in concrete mixtures are well documented in the literature [1, 31, 32, 35], only a few recent studies have investigated the effects of AEAs when incorporated into SH cementitious materials. Ersan et al. [36] studied the performance of an AEA (1% by cement mass) as a protection method for *Bacillus sphaericus* spores directly added in mortar specimens. Nevertheless, the study only reported the effects that the use of this AEA had on some of the fresh and hardened state properties of these bacteria-containing mortar samples, with no investigation conducted on the SH efficiency or spores' viability. Similarly, Luo et al. [37] proposed the use of an AEA (Eucon AEA-92) to create extra air voids that will facilitate the housing of fungal spores in cementitious SH materials. However, this study only focused on the effect that different AEA contents (between 1 mL to 2.6 mL/kg of cement) have on the pore size of cement paste specimens, with no additional investigation conducted on the SH performance. Stuckrath et al. [38] investigated the influence of an AEA on the performance of SH in reinforced mortars, where the healing agents consisted of expanded clay particles impregnated with either a precursor (i.e., calcium lactate), a biological solution (i.e., *B. pseudofirmus* cells and yeast extract) or a combination of both. It was observed that the use of AEA had no significant influence on the performance of the SH agents, while its potential use as a bacteria carrier was not investigated.

Recent studies have focused on investigating the use of AEAs as a protection method for vegetative bacterial cells directly added with the mixing water. In this regard, Bundur et al. [29] studied the use of an ammonium salt-based AEA (BASF MasterAir 200) as a protection method to improve the survival of *Sporosarcina pasteurii* vegetative cells in cement-based mortars (0.2% by cement mass). They concluded that there was a decrease in viable cell concentration due to the working mechanisms of the AEA. Nevertheless, it was concluded that the results observed were promising should spores be used instead of vegetative cells. Parastegari et al. [39] investigated the influence of the addition of vegetative *S. pasteurii* cells on the improvement of electrical resistivity and chloride penetration of air-entrained concretes. Different air content percentages (5% to 8%) and three curing media were used (water, seawater and a solution of calcium lactate

and urea), but self-healing was not investigated. More recently, Chen et al. [40] evaluated the capability of a novel AEA, containing triterpenoid saponins as its main chemical composition, to improve the viability of *S. pasteurii* vegetative cells directly added with the mixing water to heal cracks up to 0.4 mm width. Four different AEA contents (between 0.005% and 0.020% by mass of binder) were investigated. It was concluded that when vegetative *S. pasteurii* cells in a concentration of 2x 10^6 cells/mL and an AEA content of 0.01% cementitious material were used, the best flexural strength regain was achieved and the crack was successfully sealed. Nevertheless, the above-mentioned studies only evaluated the effects of AEAs when vegetative bacterial cells were directly added or when spores were encapsulated into a porous particle. None of them has specifically investigated the use of AEAs as a viable protection mechanism for directly added bacterial spores in BBSH mortars.

This study investigated the feasibility of using AEAs to protect spores in BBSH mortars to induce the healing of ~0.5 mm cracks appearing at early (28 days) and later ages (9 months). The main criteria used to define the AEAs was the chemical composition (different active surfactants), but also that these could be considered relatively inexpensive and accessible worldwide. As concrete structures are designed based on 28 days specimen strength, most published studies evaluating the healing performance of early cracks in cementitious materials have considered a 28-days curing period [19, 41-45]. On the other hand, few recent studies have evaluated the healing of cracks formed at later ages [42, 44, 46]. For example, MICP healing of older samples (i.e., 9 months old) has only been investigated by Wiktor and Jonkers [47] and Skevi et al. [48]. To evaluate the protection efficiency of these AEAs at those cracking ages, equivalent mortar specimens were also cast using a successfully proven protection mechanism (i.e., aerated concrete granules) [19]. Additionally, the influence of these AEAs on the fundamental functional properties of mortar (i.e., air contents, compressive and flexural strength, and flowability) was evaluated. A brief economic evaluation was conducted to confirm the cost-benefit associated to the use of AEAs as the protection mechanism of bacterial spores in BBSHCs.

The novelty of this study is that for the first time, the healing performance when using AEAs to purposely protect directly added bacterial spores in SH cementitious materials has been investigated and compared to other successful protection mechanisms. Even though the use of AEAs has been proposed in the past [29, 36, 37, 40] no research has specifically investigated the healing efficiency and feasibility when AEAs are used as the protection mechanism of bacterial spores directly added to SH cementitious materials. Furthermore, this study investigates for the first time the healing performance when fresh cracks are formed on 9-months-old BBSH mortars.

2. Materials and methods

2.1. *Bacterial species and growth media (GM)*

Alkaliphilic *Bacillus cohnii* DSM 6307 was obtained from the German Collection of Microorganisms and Cell Cultures (DSMZ) (Braunschweig, Germany) and stored in 25% (v/v) glycerol at -80°C. It was routinely cultured in lysogeny broth (LB) mixed with 100mL/L Na-sesquicarbonate (42 g/L $NaHCO_3$ and 53 g/L Na_2CO_3 anhydrous) to obtain pH 9.5. Spores were grown in sporulation medium [49] and harvested by centrifugation (3800 × g for 10 min) when most vegetative cells had formed spores that appeared bright when assessed with phase-contrast microscopy (48-72 hours). The spore pellet was rinsed thrice with 10 mM Tris-HCl buffer (pH 9) followed by chlorohexidine digluconate treatment (0.3 mg/mL, 30 min) to kill vegetative cells and then washed thrice as before. Spore pellets were frozen at -80°C overnight and then freeze-dried under vacuum overnight. Spore viability (cfu/g dry weight) was determined by dilution plating.

Calcium nitrate (5% of cement mass) and yeast extract (1% of cement mass) comprised the growth media (GM) used in this study. Both calcium nitrate and yeast extract were obtained from Sigma-Aldrich Corporation (UK). The GM were either added directly with mixing water or encapsulated into aerated concrete granules (ACGs) depending on application.

2.2. *Protection methods for bacterial spores*

2.2.1. Air-entraining admixture (AEA)

Three different AEAs, commonly used in concrete industry, were used in this study: Cemex Centrament Air 201, BASF MasterAir 119 and BASF MasterAir 130, and referred hereinafter as C201, B119 and B130, respectively. The dose used for each of these AEAs was determined according to the recommended dose given by the manufacturer. The recommended doses and properties of the AEAs are shown in **Table 1**.

Table 1: Chemical and physical properties of the AEAs according to manufacturers.

	Centrament Air 201	**MasterAir 119**	**MasterAir 130**
Manufacturer	Cemex Admixtures	BASF	BASF
Acronym used in this study	C201	B119	B130
Type of surfactants	Anionic	Anionic	Blend of anionic and nonionic
Surfactants	Alcohols, C12-14, ethoxylated (Laureth-4); 2-Octyl-2H-isothiazol-3-one (Ochthilinone); and lignosulphonates (for colour), chloromethyl-/methylisothiazolone and bronopol (preservatives)	Sulfonic acids, C14-16-alkane hydroxy and C14-16-alkene, sodium salts (Sodium (C14-16) olefin sulfonate); Potassium hydroxide and Rosin (Natural resin)	Sulfonic acids, C14-16-alkane hydroxy and C14-16-alkene, sodium salts (Sodium (C14-16) olefin sulfonate); Sulfuric acid, mono-C10-16-alkyl esters, sodium salts (Sodium Lauryl sulfate); Sodium hydroxide
pH Value	9.8 ± 1	10.5 ± 1	10.0 ± 1
Manufacturer suggested dose (mL/per kg cement)	2-15 (14*)	6*	3.5*

* AEA dose used in this study.

2.2.2. Aerated concrete granules (ACG)

Aerated concrete granules (ACGs) are a porous material resulting from the combination of natural quartz sand, lime and cement with aluminium powder as a foaming agent [50]. The ACG particles used in this study were supplied by Cellumat (Belgium) and sieved to achieve a particle size distribution between 1-4 mm. The loose dry bulk density and absorption capacity were 354 kg/m^3 and 120%, respectively [19]. ACG particles were utilised in selected mixes to encapsulate bacterial spores or as a carrier for GM (i.e., calcium nitrate and yeast extract). The encapsulation process was done independently to create either ACG particles containing spores or GM, and referred to hereinafter as ACG-S and ACG-GM, respectively. For the ACG-S particles, a concentrated bacterial spore suspension composed of only water and bacterial spores was incorporated into ACG by using a vacuum saturation technique, as fully described in [19]. To guarantee that these ACG particles were completely saturated with the bacterial suspension after the encapsulation process, the quantity of bacterial suspension used was equivalent to the total water absorption capacity of these ACG particles. Similarly, for ACG-GM particles, a concentrated solution composed of water and GM (i.e., calcium nitrate and yeast extract) was incorporated into ACG particles. After imbibing either the concentrated bacterial suspension or GM solution into ACG particles, the particles were dried overnight at 30°C. Next, the ACG particles were sealed with polyvinyl acetate (PVA; 50% (w/w)), provided by Bostik (UK). Sealed ACG particles were placed in Ziploc®-type plastic bags. The number of bacterial spores after the coating process was approximately 2.1 x 10^7 spores/g of ACG-S. For ACG-GM particles, the amount of calcium nitrate and yeast extract was 0.21 g and 0.05 g/g of ACG-GM, respectively.

2.3. *Preparation of mortar specimens*

The experimental programme was separated into three main groups. Specimens in Group I were used to evaluate the mechanical and physical properties, and for this, prismatic specimens conforming to BS EN 1015-11 (40 mm x 40 mm x 160 mm) were produced. Specimens in Group II and Group III were used to evaluate the self-healing capacity of cement mortar specimens after two different curing ages (28 days and 9 months) using 40 mm x 40 mm x 65 mm prismatic specimens. The abbreviation syntax for the mortar formulations was as follows: labelled first by the type of tests conducted on the specimens (M for 'Mechanical tests' and H for 'Healing tests') followed by the base mortar mix (R for plain mortar, C for plain mortar with direct addition of GM and R+ACG-GM for plain mortar with GM encapsulated into ACG). Then, the bacterial protection method: Ø (for no spores), SD (spores directly added without protection), C201 (Cemex CA201), B119 (BASF MasterAir 119), B130 (BASF MasterAir 130) and ACG-S (spores encapsulated into ACG). Lastly, the curing period submerged in water: 1M (28 days) and 9M (9 months). All the cement mortar mixes were prepared in triplets using Portland-limestone cement (CEM II/A-L 32.5R) and standard sand conforming to BS EN 197-1 and BS EN 196-1, respectively. For all the mixes, tap water was used to achieve a water/cement ratio of 0.5. Mixes without bacterial spores and GM were labelled as Reference after the Group classification. Details on the materials used, mix designs and the notation used throughout this paper are given in **Table 2**.

An automatic mortar mixer (Controls-Automix, UK) with a 5 L mixing bowl was used to prepare the mortar mixes. The procedure for mixing the mortars was adapted from the procedure in BS EN 196-1 as follows. Firstly, if spores or AEAs were included in the mix, these were added to the total amount of water (mixing water) and manually mixed for 30 s. Then, cement was added to the total amount of water and manually mixed for an additional 30 s. In the mixes with the direct addition of GM (i.e., calcium nitrate and yeast extract), these were added to the cement paste and manually mixed for an additional 30 s. After the initial manual mixing (90 s), further mixing was carried out using the automatic mortar mixer per BS EN 196-1 (240 s). For the mixes containing ACG particles, these were previously dry mixed with the total amount of sand. To efficiently use the spores in Group II and II specimens, the mortar specimens were cast in two layers (20 mm each). The bottom layer was cast as per the mix designs shown in **Table 2**, while the top layer consisted of plain mortar (i.e., Reference mix). The bottom layer was placed first, and after 90 min, the top layer was placed on top. Specimens were demoulded after 48 h and then cured for 28 days or 9 months submersed in tap water (20°C ± 2°C) in separate containers to avoid cross-contamination.

Table 2: Mix design and notation of all mortar samples used in this study.

Mix	Specimen dimensions (mm)	Cement (g)	Water (mL)	Standard sand (g)	Calcium nitrate (g)	Yeast extract (g)	Bacterial spores (cfu)	ACG-S (g) *	ACG-GM (g) **	AEA (mL)
M_Reference_1M	40x40x160	387	193	1160	0	0	0	0	0	0
M_C_ Ø_1M	40x40x160	387	193	1160	19.1	4.2	0	0	0	0
M_C_SD_1M	40x40x160	387	193	1160	19.1	4.2	$4.5x10^8$	0	0	0
M_C_C201_1M	40x40x160	387	193	1160	19.1	4.2	$4.5x10^8$	0	0	5.80
M_C_B119_1M	40x40x160	387	193	1160	19.1	4.2	$4.5x10^8$	0	0	2.50
M_C_B130_1M	40x40x160	387	193	1160	19.1	4.2	$4.5x10^8$	0	0	1.50
M_C_ACG-S_1M	40x40x160	387	193	1092	19.1	4.2	0	22.3	0	0
M_R+ACG-GM_ACG-S_1M	40x40x160	387	193	869.4	0	0	0	22.3	92.4	0
H_Reference_1M	40x40x65	92	46	276	0	0	0	0	0	0
H_C_ Ø_1M	40x40x65	92	46	276	4.55	1.0	0	0	0	0
H_C_SD_1M	40x40x65	92	46	276	4.55	1.0	$1.1x10^8$	0	0	0
H_C_C201_1M	40x40x65	92	46	276	4.55	1.0	$1.1x10^8$	0	0	1.40
H_C_B119_1M	40x40x65	92	46	276	4.55	1.0	$1.1x10^8$	0	0	0.60
H_C_B130_1M	40x40x65	92	46	276	4.55	1.0	$1.1x10^8$	0	0	0.35
H_C_ACG-S_1M	40x40x65	92	46	260	4.55	1.0	0	5.3	0	0
H_R+ACG-GM_ACG-S_1M	40x40x65	92	46	207	0	0	0	5.3	22.0	0
H_Reference_9M	40x40x65	92	46	276	0	0	0	0	0	0
H_C_ Ø_9M	40x40x65	92	46	276	4.55	1.0	0	0	0	0
H_C_SD_9M	40x40x65	92	46	276	4.55	1.0	$1.1x10^8$	0	0	0
H_C_C201_9M	40x40x65	92	46	276	4.55	1.0	$1.1x10^8$	0	0	1.40
H_C_B119_9M	40x40x65	92	46	276	4.55	1.0	$1.1x10^8$	0	0	0.60
H_C_B130_9M	40x40x65	92	46	276	4.55	1.0	$1.1x10^8$	0	0	0.35
H_C_ACG-S_9M	40x40x65	92	46	260	4.55	1.0	0	5.3	0	0
H_R+ACG-GM_ACG-S_9M	40x40x65	92	46	207	0	0	0	5.3	22.0	0

* ACG-S for 40x40x65 mm^3 specimens (i.e., 5.3 g) contains 1.1 x 10^8 spores while ACG-S for 40x40x160 mm^3 specimens (i.e., 22.3 g) contains 4.5 x 10^8 spores.
** ACG-GM for 40x40x65 mm^3 specimens (i.e., 22.0 g) contains 4.55 g calcium nitrate and 1 g yeast extract, while ACG-GM for 40x40x160 mm^3 specimens (i.e., 92.4 g) contains 19.1 g calcium nitrate and 4.2 g yeast extract.

2.4. *Test methods*

2.4.1. Bacterial spore viability with proposed AEAs

To determine whether AEAs had any impact on the viability of spores, they were incubated together. The concentrations of AEA, water and bacterial spores shown in **Table 2** were used after a 1/10 scaling reduction to keep weighing and pipetting volumes reasonable while reducing the number of spores needed. For each preparation, calcium nitrate (0.45 g) and yeast extract (0.1 g) were added to the water volume (4.6 mL) along with bacterial spores (3.8 x 10^7 *B. cohnii* spores) and the corresponding AEA (i.e., C201, B119 or B130) to be tested. After all the components were completely mixed, the samples were incubated for 15 minutes at room temperature. Dilution plating (incubated overnight at 30°C, LB agar pH8.2) was then used to determine viable cell counts. Plate counts of spores incubated with AEAs were compared to a control plate where spores were incubated in identical conditions in the absence of AEAs.

2.4.2. Air bubbles encapsulation

To test for the capacity of the different AEAs to successfully encapsulate bacterial spores, a defined volume of each AEA, C201 (0.70 mL), B119 (0.30 mL) and B130 (0.20 mL), was pipetted onto the bacterial spores (1.2 x

10^{10} *B. cohnii* spores) to fully coat them before adding 23 mL of a molten 1% agarose gel prepared in distilled water. This was mixed by vortex for 20 s, and then a drop of each preparation was placed onto a glass slide with a coverslip. Images were immediately obtained with a compound microscope at 100x and 400x magnification.

2.4.3. Determination of air content

The air content of the mixes was obtained using an air-entraining meter (Testing, Germany) per BS EN 1015-7 (Method A-Pressure method). The air content measurements were directly obtained from the air-entraining meter, based on the principle of air bubble compressibility [51]. The reported air content was calculated as the mean value from two individual values obtained for each mortar mix.

2.4.4. Flowability and strength response

Flowability of the mortar mixes was determined using a flow table test at a water/cement ratio of 0.5, following BS EN 1015-3. In addition, compressive and flexural strength tests were carried out for all 40 mm x 40 mm x 160 mm mortar specimens (Group I) at 28 days per BS EN 1015-11. Using a 100 kN hydraulic frame, triplets of each mortar mix were tested for flexural strength. The resulting halves (i.e., six per mix) were subsequently used for compressive strength tests.

2.4.5. Investigation of self-healing efficiency

The following three essential conditions proposed by Tziviloglou et al. [16] were considered to evaluate the BBSH efficiency of the mortar specimens: (i) proof of bacterial activity, (ii) recovery of the water penetration resistance as the crack healed and (iii) precipitation of mineral crystals within the crack. In this context, the recovery of water tightness was evaluated through water-flow tests, while precipitates formed within the cracks were analysed using an electronic microscope and crack area quantification using commercial software (ImageJ). In addition, SEM-EDX and Raman spectroscopy were used to confirm bacterial activity.

After curing for 28 days submerged in water, all the 40 mm x 40 mm x 65 mm specimens (Group II) were dried at room temperature for 24 h, while a similar process was carried out for specimens of Group III after 9 months of curing. For all Group II and Group III specimens, first, a notch of approximately 1.5 mm depth was sawn at the centre of each specimen to induce the crack formation within this notch. Then, the top half of the specimens was wrapped with carbon fibre-reinforced polymer strips to guarantee the integrity of the sample. Specimens were cracked by three-point bending using a 100 kN hydraulic frame. The load was applied to maintain a crack growth of 0.025 mm/min, and loading was stopped when the crack width was sufficiently large to allow the placement of two 0.5 mm thick plastic spacers at both ends of the formed crack. Once the plastic spacers were placed, the load was slowly removed. Two selected crack locations were marked with a permanent marker to enable monitoring of the crack width healing at the same location. After cracking, all the mortar specimens were placed in plastic containers (one for each mix and Group) that were open to the atmosphere, with the main crack facing upwards and filled with tap water to 10 mm below the top of the specimens. The specimens were then incubated at 20°C for 56 days and periodically inspected. Prior to the periodic visual observation of the cracks, mortar specimens were removed from the water and left to dry at air exposure for 2 h under laboratory conditions (20°C) to obtain an unwetted crack surface. Other researchers have recommended this pre-conditioning of the samples to avoid odd brightness effects due to the presence of water in the crack when analysed under the microscope lights [52, 53]. Visualisation of crack healing was monitored using a Celestron (USA) portable microscope. Images were taken immediately after cracking and at 7, 28 and 56 days of healing. Image binarization was conducted to determine the healing ratio using the commercially available image processing programme ImageJ [54, 55]. Pixels in the crack area were counted before and after healing by defining a black threshold level of 100. Similar threshold values have been used in similar studies when using this binarization method [56]. The healing ratio was measured as the decrease in the fraction area of each crack identified by black pixels corresponding to the cracks in the photos taken immediately post-cracking and at the final age (i.e., 56 days). The mean healing ratio (HR) was calculated according to **equation 1**:

$$\text{Mean Healing Ratio (HR)} = \frac{1}{n}\sum_{1}^{n}\frac{(A_i - A_f)}{A_i} \text{ x } 100\% \quad (1)$$

where A_i and A_f = initial and final area (respectively) of the complete crack of an individual mortar specimen, and n = total number of mortar samples analysed per mix. The use of image binarization to quantify crack areas when investigating self-healing cementitious materials has previously been shown to accurately identify the crack and calculate its area with high precision [55, 56].

Additionally, for each mortar specimen, three crack widths (in millimetres) were taken at the same location in the two different points previously marked with a permanent marker (six measurements per sample) at different healing times (post-cracking, 7, 28 and 56 days). The mean crack width for the complete crack was calculated by averaging these six measurements, while the healing (crack closure) percentage was calculated for each location according to **equation 2**:

$$\text{Healing (crack width) \%} = \frac{(Cw_i - Cw\,t)}{Cw_i} \times 100 \quad (2)$$

where Cw_i = initial crack width, and Cw_t = width measured at the time t.

A water-flow test, based on RILEM test Method 11.4 [57], was used to calculate the recovery of the water penetration resistance of the mortar specimens as the crack healed. Tests were carried out immediately after cracking and at 28 and 56 days of healing. The water-flow coefficient, k, was calculated according to **equation 3** [19]:

$$k = \frac{aL}{A_t} \ln\left[\frac{h_1}{h_2}\right] \quad (3)$$

where k = water-flow coefficient (cm/s); a = cross-sectional area of the cylinder (1.8 cm^2); L = depth of mortar specimen (4 cm); A = cross-sectional area of the acrylic plate (10.2 cm^2); t = time (s); h_1 = initial water head (12.4 cm); and h_2 = final water head (cm). The healing percentage was calculated according to **equation 4**.

$$\text{Healing percentage (\%)} = \frac{(k_0 - k_t)}{k_0} \times 100 \quad (4)$$

where k_0 = initial water-flow after cracking and k_t = water-flow at healing time t.

2.4.6. Microstructural analysis

Microstructural analysis was performed for H_C_ Ø, H_C_ACG-S and H_C_C201 representative mortar specimens after 56 days of healing. From the three different mixes containing AEAs, only H_C_C201 mortar specimens were analysed as this was the AEA mix that overall achieved the best SH performance. Before conducting the microstructural analyses, all the specimens were oven-dried for seven days at 40°C. For scanning electron microscope (SEM) analyses, the mortar specimens were placed in an E306 vacuum coating system (Edwards, UK) until they were outgassed. Backscattered Electron (BSE) images were obtained using a SU-3900 large chamber SEM (Hitachi, Japan). The SEM system was set at 20 keV accelerating voltage and an 86 µA beam current. Energy Dispersive X-ray (EDX) analyses were conducted to detect the elemental composition of the healing products formed within the cracks. The EDX spectra were acquired using a 170 mm^2 UltiMax (Oxford Instruments, UK) detector at 20 keV accelerating voltage and accumulated over a 50-sec interval. Raman spectroscopy analyses were used to identify the chemical structure of the healing products. Raman spectra were acquired using an InVia confocal Raman microscope (Renishaw, UK) with a laser wavelength of 532 nm. Raman spectra were acquired in 10 accumulations of 10 s each in a spectral window of 100-1860 cm^{-1}. The spectra were background corrected.

3. Results

3.1. *Bacterial spore viability with proposed AEAs*

The impact of AEAs on spore viability was tested by co-incubating spores and AEAs and then plating dilutions to monitor viable counts. **Fig. 1** shows the growth of *B. cohnii* colonies on LB media (pH 8.2) following incubation with the AEAs used in this study compared to a positive control (without AEA). Similar cell

viabilities were observed when AEAs were compared to the positive control, suggesting that none of the AEAs have a significant impact on the viability or germination efficiency of these bacterial spores.

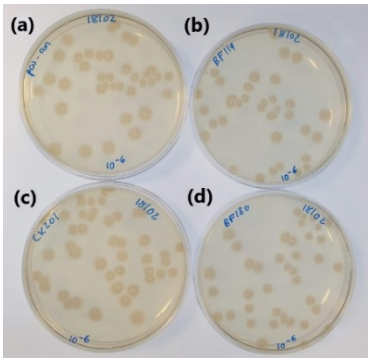

Fig. 1. Representative plates **(a)** Positive control, **(b)** B119, **(c)** C201 and **(d)** B130) for 10^{-6} dilution showing bacterial colonies (*B. cohnii*) grown on LB media (pH 8.2) following 15 min incubation with the AEAs.

3.2. *Air bubbles visualisation*

A visual inspection was carried out to validate if the spores could be successfully encapsulated within the micro-bubbles created when these AEAs are used (**Fig. 2**). When different suspensions containing AEA and bacterial spores were independently added to agarose gel and briefly vortexed, a high concentration of bacterial spores was observed inside the micro-bubbles, with only very few spores remaining outside the micro-bubbles. In contrast, no micro-bubbles were formed when a bacterial spore suspension without AEA was added to the molten agarose and vortexed. These results show that the micro-bubbles produced by the addition of AEAs were able to successfully entrap significant numbers of bacterial spores and maintain them within the micro-bubbles' void space upon mixing with agarose.

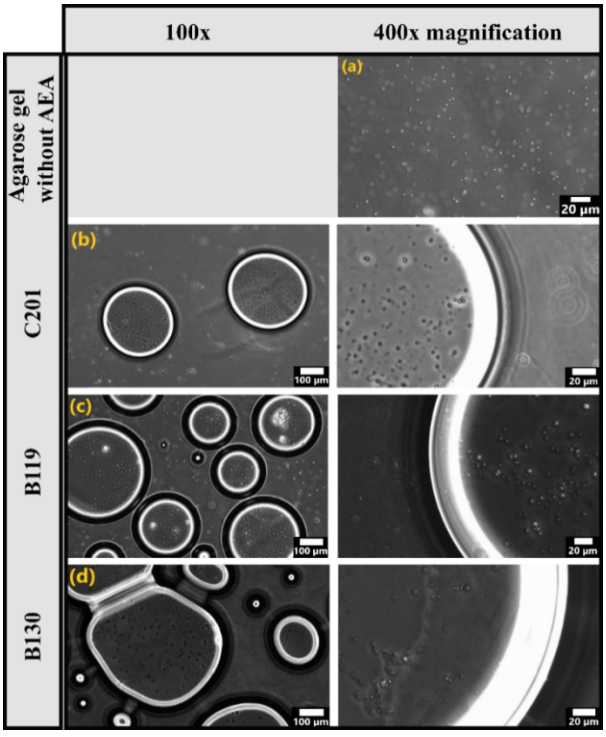

Fig. 2. Microencapsulation of *B. cohnii* spores with AEAs in 1% agarose gel. A defined volume of each AEA was pipetted onto 1.2 x 10^{10} spores before adding a molten agarose gel prepared in distilled water: **(a)** Control

agarose gel (without AEA), **(b)** C201, **(c)** B119 and **(d)** B130. At 100x magnification, bacterial spores are visible inside the micro-bubbles (black and white framed circles). At 400x magnification, a section of these micro-bubbles is shown where a high concentration of bacterial spores can be observed within the void space while few spores are visible in the agarose gel outside the micro-bubble. No micro-bubbles were formed when bacterial spores (without AEA) were added to the agarose gel and vortexed.

3.3. *Fresh and hardened state properties of mortar*

Fig. 3 shows the results of the air content and flowability measurements for the different mixes used in this study. The air content observed for the Reference mix (5.2%) is within the range of values reported in other studies for similar mortar mixes (i.e., 5.0-5.7% air content) [16, 51]. Mixes containing AEAs presented a four-fold increased air content value compared to the Reference mix, but only two-fold air contents compared to the rest of the mixes without AEAs and where GM was directly added. It was observed that the direct addition of yeast extract (1% of cement mass) in the M_C_Ø mix led to a 115% increase in air content when compared to the Reference mix. Other researchers have reported similar increases in air content when yeast extract is used in mortar mixes [58]. In contrast, the air content observed was similar to the Reference mix when the GM was incorporated *via* encapsulation (i.e., M_R+ACG-GM_ACG-S). It can be observed that regardless of the different doses added, the air contents of the three AEA mixes were very similar. As expected, a trend of increasing flowability with increasing air content was observed due to the lower plastic viscosity of air-entrained cement mortars [34, 59]. The addition of yeast extract created a more liquid fresh mixture with increased air content when compared to the reference mix, which other researchers have previously reported [16]. Note that the air content used for the AEA mixes was high in order to maximise the protection of spores and was much higher than would be used to provide resistance to freeze/thaw attack [34].

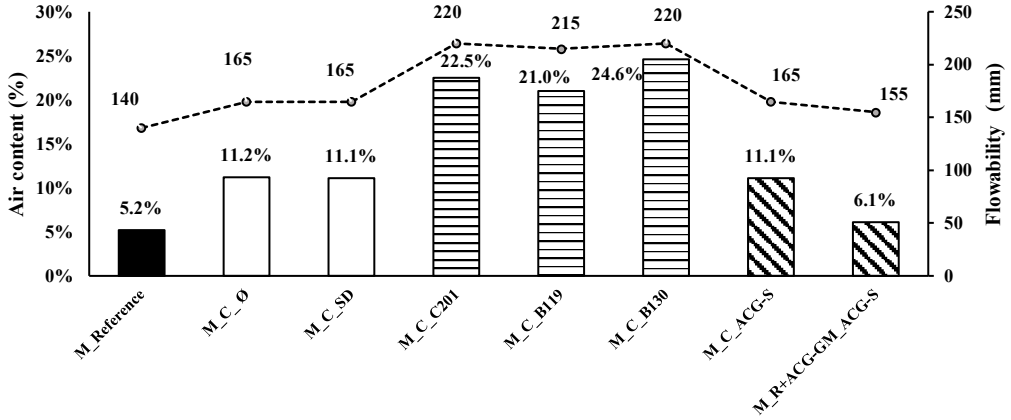

Fig. 3. Air content (%) and flowability (mm) of the different mortar mixes. (■) Reference mix, (□) Control mixes (with and without spores), (▤) mixes containing AEAs and (▧) mixes containing ACG particles.

The addition of AEAs caused a significant decrease in the compressive and flexural strength response (after 28 days of curing) of the order of ~56% and ~48%, respectively (**Fig. 4**). The percentage of strength change, Δ%, of the different mixes compared to the Reference mix are given in **Fig. 4**. The AEA mixes presented a compressive strength decrease of 3.19% per unit air increase, which is consistent with values elsewhere [59, 60]. The strength decrease observed was principally due to the additional air voids within the mortar matrix formed by the AEA. However, part of this strength decrease was also caused by the direct addition of yeast extract (present in the GM), likely related to the formation of micro-bubbles [36, 58, 61]. Furthermore, for the mortar mixes M_C_ACG-S and M_R+ACG-GM_ACG-S, where the sand was partially replaced by ACG particles, the compressive strength decreased due to these weaker particles by 6.6% and 37.8%, respectively, when compared to equivalent mixes without ACG particles replacements (i.e., M_C_Ø and M_Reference).

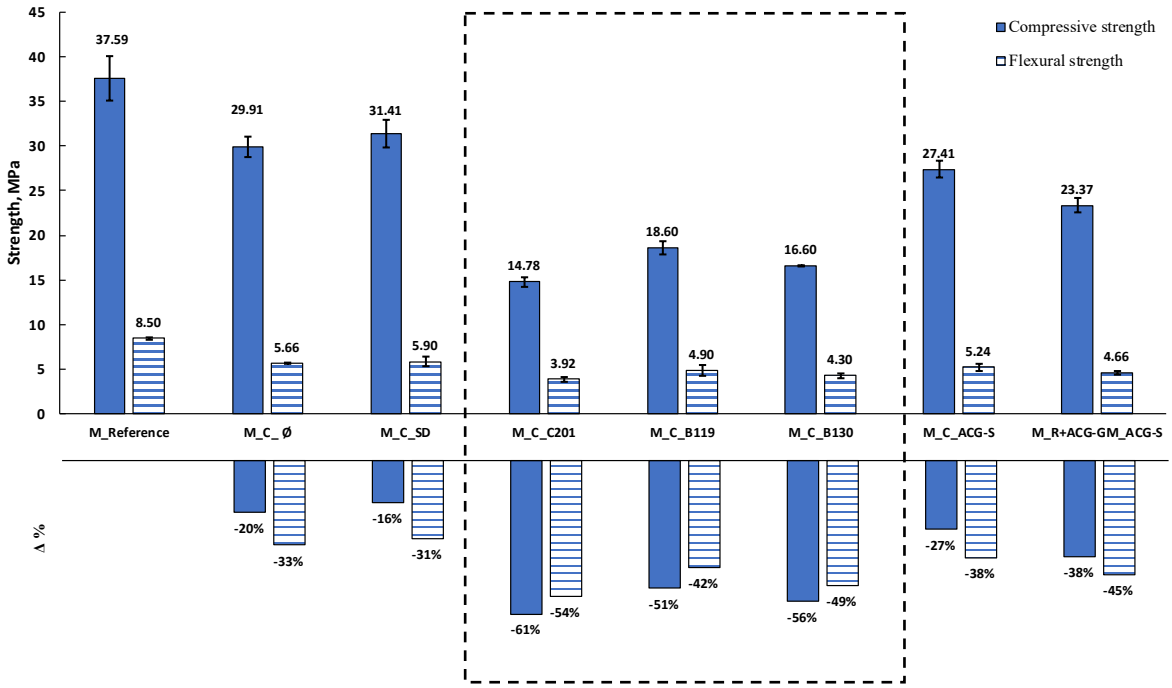

Fig. 4. Compressive and flexural strength of Group I mixes after 28 days of curing and the percentage variation of the strength, Δ%, of all the mixes compared to the Reference mix. Mixes containing AEAs are shown inside the dotted box. Error bars represent ± one standard deviation.

3.4. *Self-healing efficiency*

This study employed two healing ratio parameters: crack area quantification and water-flow tests. Crack area quantification is quick and non-destructive, while water-flow tests are essential to evaluate the recovery of permeability properties [53].

3.4.1. Crack area quantification

Images of the complete crack for each specimen were taken with a digital microscope immediately after cracking and after 28 and 56 days of healing (incubation period). Using commercial photo editing software, the complete crack image was created by overlapping individual images. Each of the individual images represented an area of 9.6 x 7.2 mm with a resolution of 5.0 Megapixels. This resolution (i.e., each pixel equivalent to 3.7 μm) was kept up for the composed images. The composed images were processed using ImageJ software to obtain the complete crack binarization image for each specimen. **Figures 5** and **6** show the composed and binarization images of a complete crack, immediately after cracking and after 56 days of healing, for a representative specimen of each mix of Groups II and III, respectively.

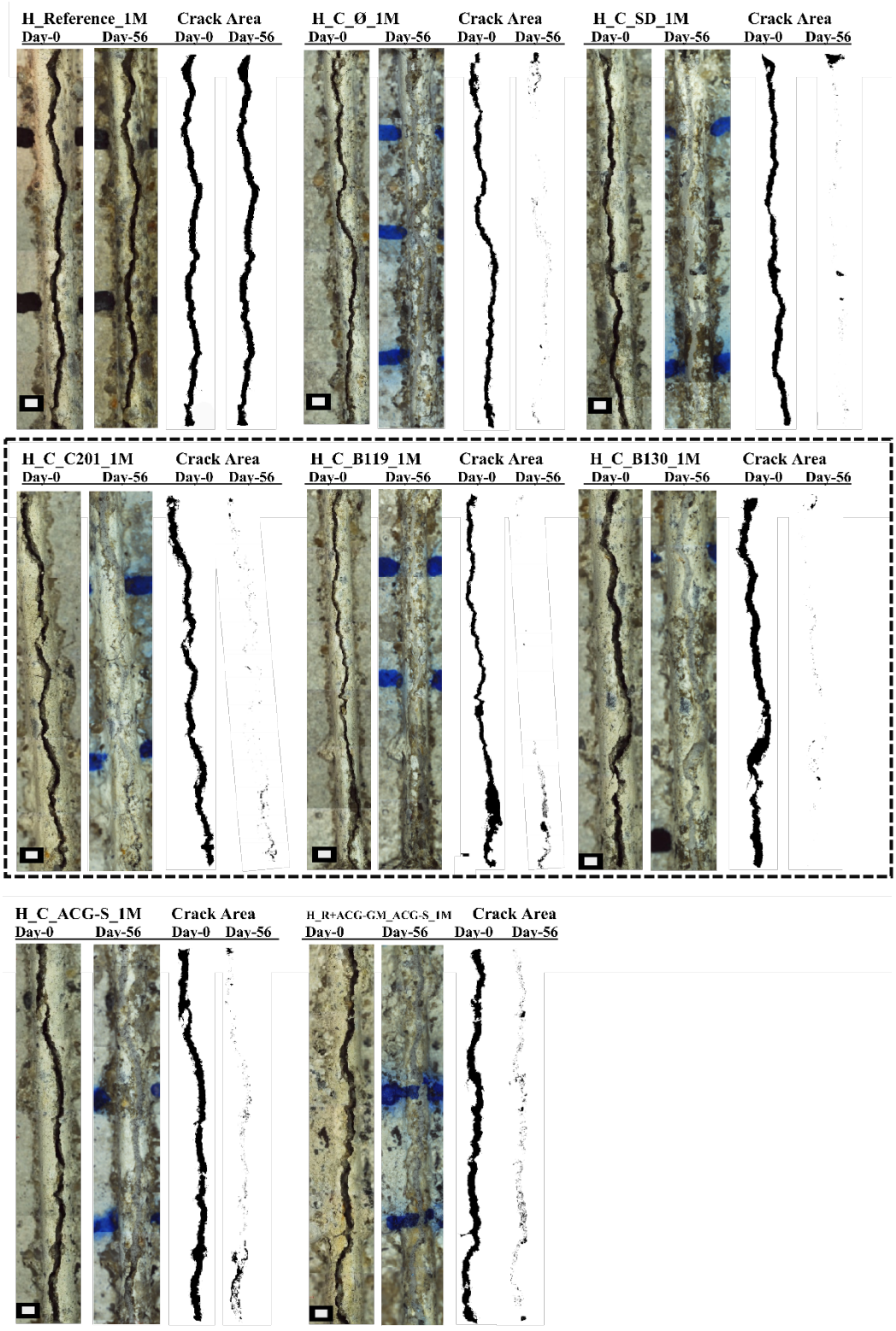

Fig. 5. Composed and binarization images are shown for a representative specimen of each mix tested from Group II (28-days curing) immediately after the cracking process and after 56 days of healing. Mixes containing AEAs are shown inside the dotted box. Scale bars represent 1.0 mm.

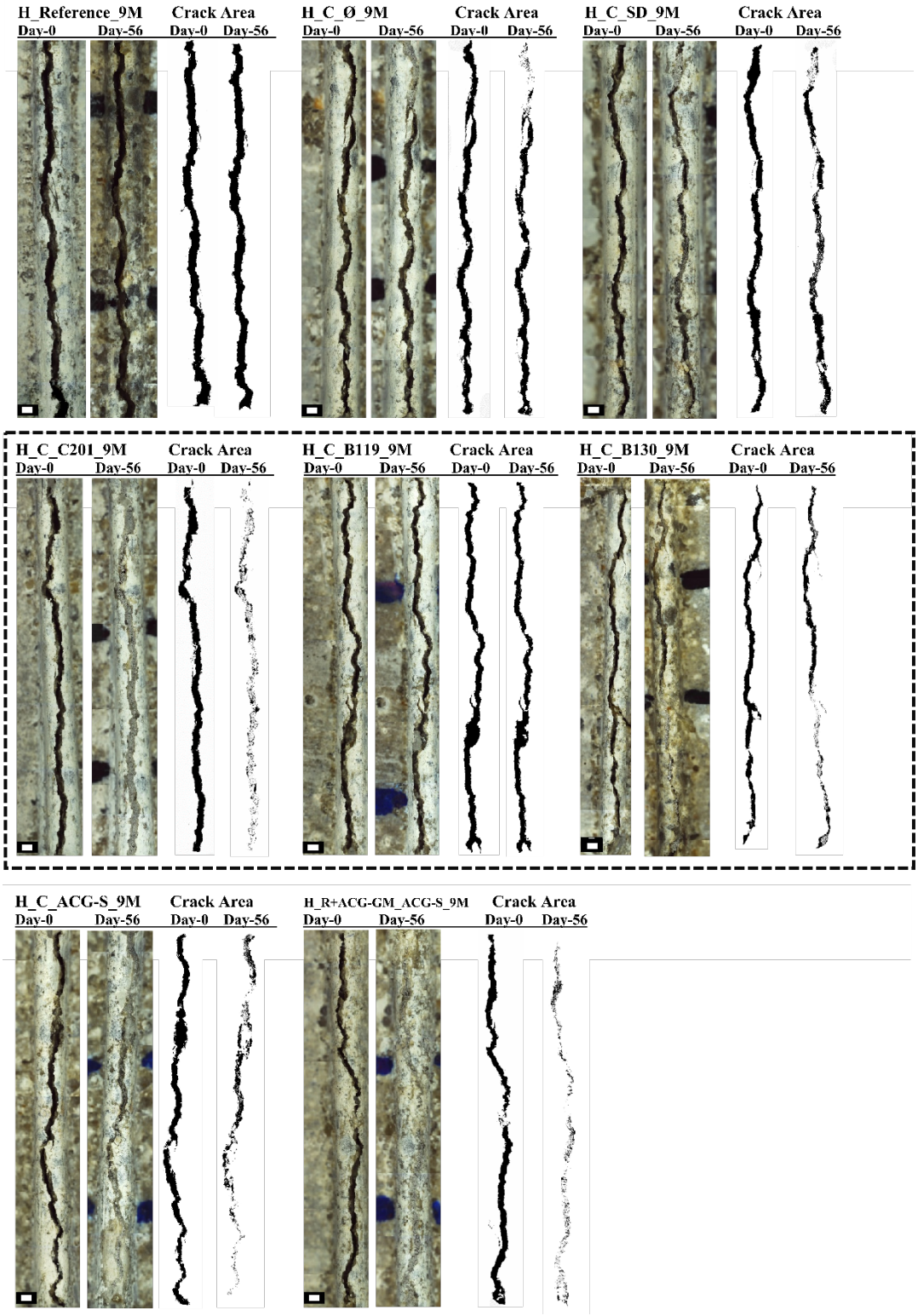

Fig. 6. Composed and binarization images are shown for a representative specimen of each mix tested from Group III (9-months curing) immediately after the cracking process and after 56 days of healing. Mixes containing AEAs are shown inside the dotted box. Scale bars represent 1.0 mm.

Fig. 7 shows the healing ratio (HR) obtained from the area quantification for Groups II and III mortar specimens. Important to mention is that the reference mixes (without bacterial spores and no GM added)

behaved similarly in both situations (i.e., HR below 10%), while the control mixes (H_C_Ø_1M and H_C_Ø_9M), without bacterial spores but containing GM added directly with the mixing water, showed a high HR% when cracked at 28 days but very low healing efficiency when specimens of the same mix were cracked after 9 months of curing (*left dotted box*, **Fig. 7**). Furthermore, the mix where the GM and the bacterial spores were encapsulated independently into ACG particles presented the same HR behaviour irrespectively of the age when the crack was formed (*right dotted box,* **Fig. 7**).

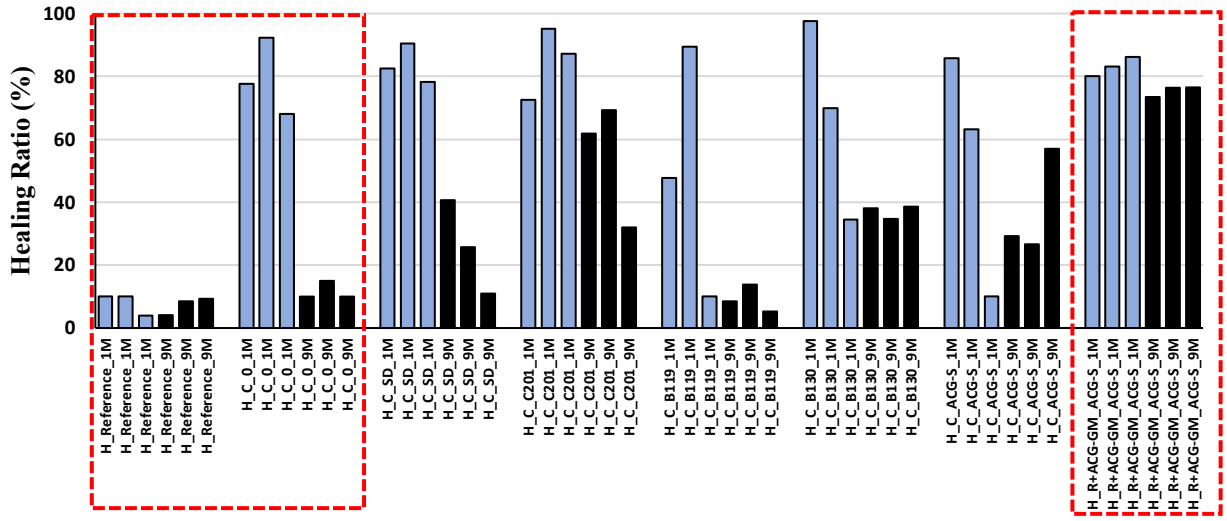

Fig. 7. Healing ratio percentage (HR%) obtained from the complete crack binarization images for Groups II and III specimens after 56 days of healing. Bars represent individual mortar specimens as: (■) Group II (28-days cracking) and (■) Group III (9-months cracking). The *left dotted box* shows the two mortar mixes without bacterial spores, and the *right dotted box* shows the mortar mix where bacterial spores and GM were independently encapsulated into ACG.

Three crack width measurements were taken at fixed locations (top, middle and low section of the crack) within the crack in each of the two points marked with a permanent marker of each specimen. In total, 18 measurements were performed for each mix of each Group (288 total measurements). These measurements were taken immediately after cracking and then after 7, 28 and 56 days of healing. **Table 3** shows the mean crack width calculated by averaging the measurements of the three specimens of each mix (18 measurements) immediately after cracking (before healing).

Table 3. Mean crack width for mortar specimens of Group II and III.

	Mean crack width (mm)	
Mix	**Group II***	**Group III****
H_Reference	0.44	0.49
H_C_Ø	0.47	0.51
H_C_SD	0.49	0.54
H_C_C201	0.47	0.51
H_C_B119	0.43	0.48
H_C_B130	0.59	0.49
H_C_ACG-S	0.55	0.56
H_R+ACG-GM_ACG-S	0.60	0.48

*. Cracking after 28 days of curing
**. Cracking after 9 months of curing

However, as crack widths can vary significantly along the length of a single crack, it is not advisable to compare crack mean widths to evaluate the healing performance of these cracks [47]. In this context, crack healing percentage as a function of the initial crack width was calculated by measuring the crack widths at the same specific locations after different healing times. Results are shown in **Fig. 8 (A)** and (**B)** for Group II and III specimens, respectively.

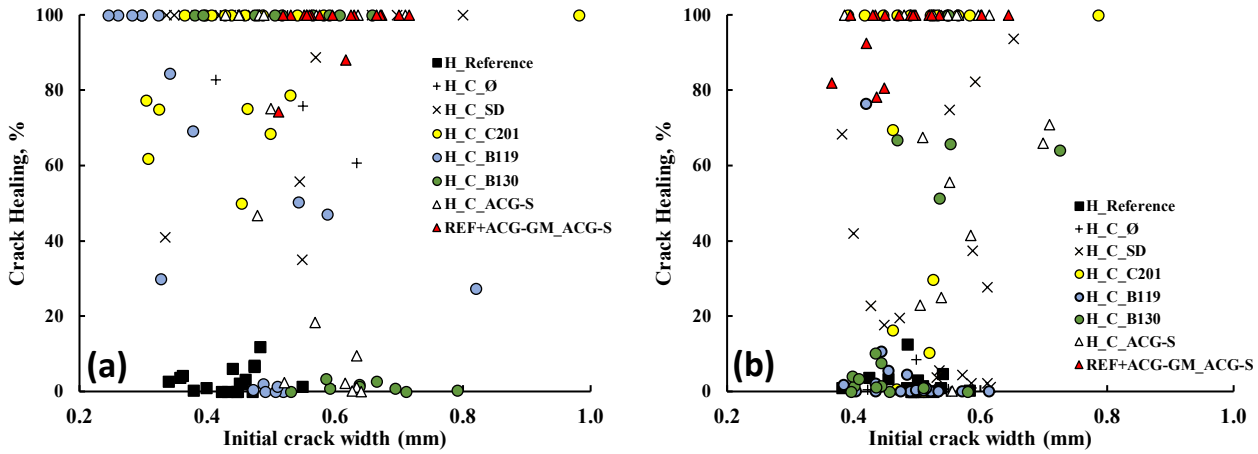

Fig. 8. Crack healing (%) as a function of the initial crack width for specimens of: **(a)** Group II and **(b)** Group III. 18 measurements are plotted for each mix after a healing time of 56 days (144 total measurements per Group). Specimens were cracked after a curing period of 28 days or 9 months for Group II and Group III, respectively.

3.4.2. Water-flow tests

Water-flow tests were conducted immediately after the cracking process (as the reference value) and after 28 and 56 days of healing. As suggested by Roig-Flores, et al. [53], intermediate measurements (i.e., 7, 14 and 21 days) were not performed to avoid uncontrolled effects that could result in the removal of newly formed precipitates (**Fig. 9**), affecting healing performance.

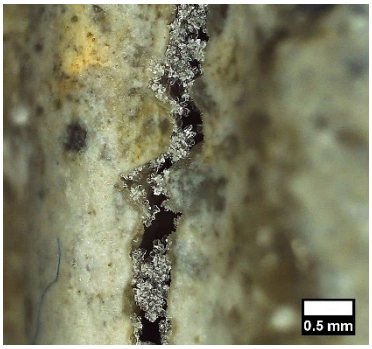

Fig. 9: Digital microscope image of a crack in a mortar specimen (H_C_SD) showing newly formed $CaCO_3$ crystals after seven days of healing.

The percentage of crack healing as a function of reduction in the water-flow coefficient after 56 days of healing for mortar specimens of each mix is shown in **Fig. 10**. These results were generally consistent with the decrease in the crack area observed with the microscopy and measurements of crack width closure.

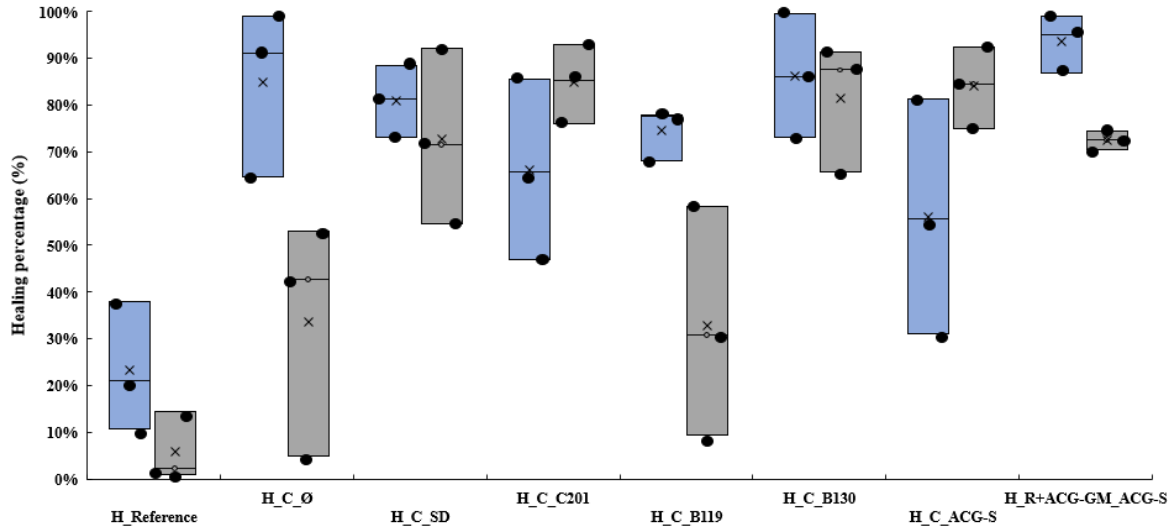

Fig. 10: Boxplot of the healing percentage (%) as a function of reduction in the water-flow coefficient after 56 days of healing for mortar specimens cracked at 28 days (Group II (■ bars)) and 9 months (Group III (■ bars)). For each mix, individual measurements and mean values are represented by circles and crosses, respectively. The median value is represented by the middle bar, while the bottom and top bars represent the minimum and maximum value of each mix, respectively.

3.5. *Microstructural analyses*

The microstructure of healed cracks was investigated using SEM-EDX and Raman spectroscopy on Group II and Group III representative mortar specimens after 56 days of healing. Specimens of the AEA-containing mortar mix that presented the best SH performance (i.e., H_C_C201) were analysed to investigate the chemical structure and morphology of the healing products. Additionally, H_C_ Ø and H_C_ACG-S specimens were analysed for comparison purposes.

SEM and EDX– As shown in **Fig. 11,** different crystals morphologies were observed depending on the time of the cracking for H_C_C201 specimens. The SEM image (**Fig. 11(a)**) shows a layer of white precipitates almost completely closing the crack of around 0.50 mm in width. The microcrack observed likely resulted during SEM analysis, probably due to desiccation and drying shrinkage that is likely to occur during the preparation of the sample [62]. When the specimens were cracked at an early age (28 days), the crystals were distributed in a deformed actinomorphic form **(Fig. 11(b)**) that differed from the rhombohedra-like deformed crystals observed in the 9-months-cracked specimens (**Fig. 11(c)**). In this regard, even though the initial amounts and type of calcium precursor (calcium nitrate), nutrients (yeast extract) and bacterial spores (*B. cohnii*) used for the H_C_C201 specimens of both groups (Group II and Group III) were the same and the environmental curing conditions very similar, the age of the mortar specimen at the time of cracking could have likely produced different cement matrix conditions that affected the morphology of the crystals formed. For the deformed actinomorphic morphology of the precipitates observed in the H_C_C201_1M specimen, a possible explanation could be the likely higher amount of nitrogen present in the cement matrix coming from the calcium precursor (i.e., calcium nitrate) when the crack was formed at an early age (28 days). Yan-Rong *et al.* [63] observed that the addition of triethanolamine (TEA), an organic compound containing nitrate, considerably altered the crystalline phase and morphology of calcium crystals from large and lamellar shapes to smaller and deformed actinomorphic ones, similar to the ones observed in this study. In contrast, the distinct rhombohedra-like deformed crystals observed in H_C_C201_9M (**Fig. 11(c))** appear very similar to bacterially mediated morphologies described in several reported studies [47]. Moreover, closer examination of the healing products revealed surface bacterial imprints that likely corroborate the microbial origin of these precipitates (**Fig. 11(d)**).

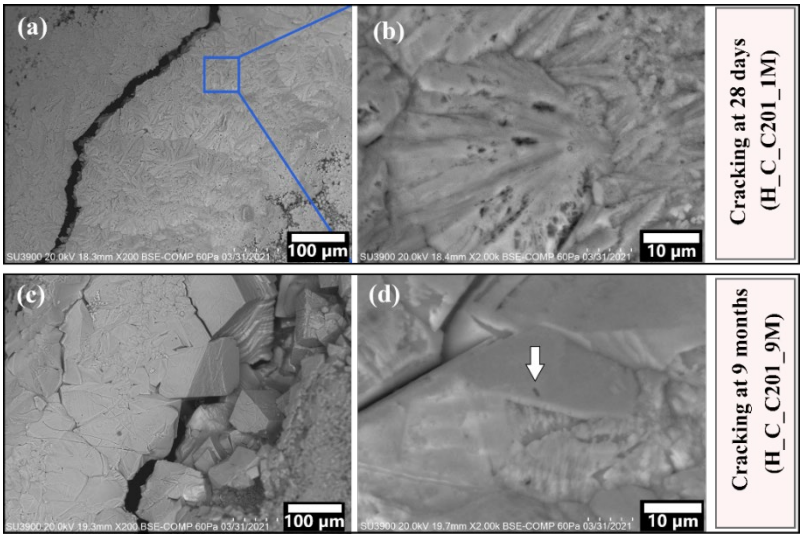

Fig. 11. Calcite crystals observed through SEM analysis of the H_C_C201 mortar specimens (Group II and III) after 56 days of healing. **(a)** for H_C_C201_1M, **(b)** for H_C_C201_1M detail of the deformed actinomorphic shape of the precipitates in H_C_C201_1M, **(c)** for H_C_C201_9M, and **(d)** for detail of calcite crystal with surface bacteria imprint (indicated by arrow) in H_C_C201_9M.

The H_C_C201 SEM results were compared to the control specimen (H_C_Ø) and to the specimen cast using the self-healing mix previously proved by the authors to be successful (H_C_ACG-S) [19, 41]. **Fig. 12** shows SEM images for the H_C_Ø_1M (**(a)**, **(b)**), and H_C_ACG-S_9M specimens (**(c)**, **(d)**).

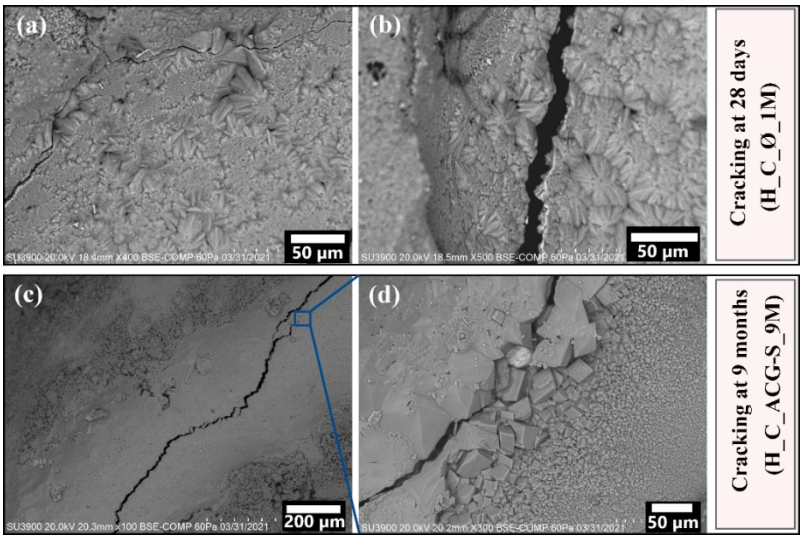

Fig 12. Healing products observed through SEM analysis of the H_C_Ø_1M and H_C_ACG-S_9M after 56 days of healing. **(a)** for crack area of H_C_Ø_1M showing the deformed actinomorphic shape of the precipitates, **(b)** for crack detail of H_C_Ø_1M, **(c)** for closed crack in H_C_ACG-S_9M, and **(d)** calcite crystals observed in the crack of H_C_ACG-S_9M.

Crack widths of around 0.50 mm were completely filled with calcium carbonate precipitates for the control specimens without bacteria but with GM that were cracked after curing for 28 days (H_C_Ø_1M). However, no sign of calcium carbonate precipitation was observed when specimens of this same mix were cracked after 9 months (H_C_Ø_9M). SEM observations of H_C_Ø_9M are therefore not included in this section. The

healing products observed in the cracks of H_C_Ø_1M specimens (**Fig. 12(a), (b)**) presented the same deformed actinomorphic forms as the ones found in H_C_C201_1M specimens (**Fig. 11(a), (b)**). In contrast, the healing products observed for H_C_ACG-S_9M presented distinctly rhombohedral-shaped crystals commonly associated with calcite precipitates (**Fig. 12(d)**) like the ones observed in H_C_C201_9M specimens.

EDX analyses, conducted on the precipitates formed within the cracks of H_C_C201_1M (**Fig 13(a)**) and H_C_C201_9M specimens (**Fig 13(b)**), presented three main elements: C, O and Ca, corroborating that the mineral precipitates were $CaCO_3$-based. EDX analysis conducted away from the crack area (***Spectrum 3*** of **Fig. 13(c)**) showed a significant high peak associated with Si and minor peaks associated with Fe and K, which are consistent with standard Portland cement matrix observed in other studies [64, 65]. While the precipitates in H_C_C201_1M presented an actinomorphic form that significantly differed from the morphology commonly observed for calcium carbonates, as explained above, the EDX analysis (***Spectrum 1***) showed high calcium amounts along with C and O, similar to those observed for H_C_C201_9M (***Spectrum 2***). This confirms the presence of calcium carbonate precipitates healing the cracks of H_C_C201_1M. As shown in **Fig. 13(d),** the EDX spectrum for the precipitates of the H_C_ACG-S_9M specimen (***spectrum 4***), where the bacterial spores were encapsulated into ACG particles instead of using an AEA, presented very similar peaks for C, O and Ca as the ones observed in the H_C_C201 specimen. Therefore, EDX analyses prove that the main precipitates within the cracks of H_C_C201 specimens that have been cracked, either at 28 days or 9 months, are $CaCO_3$-based.

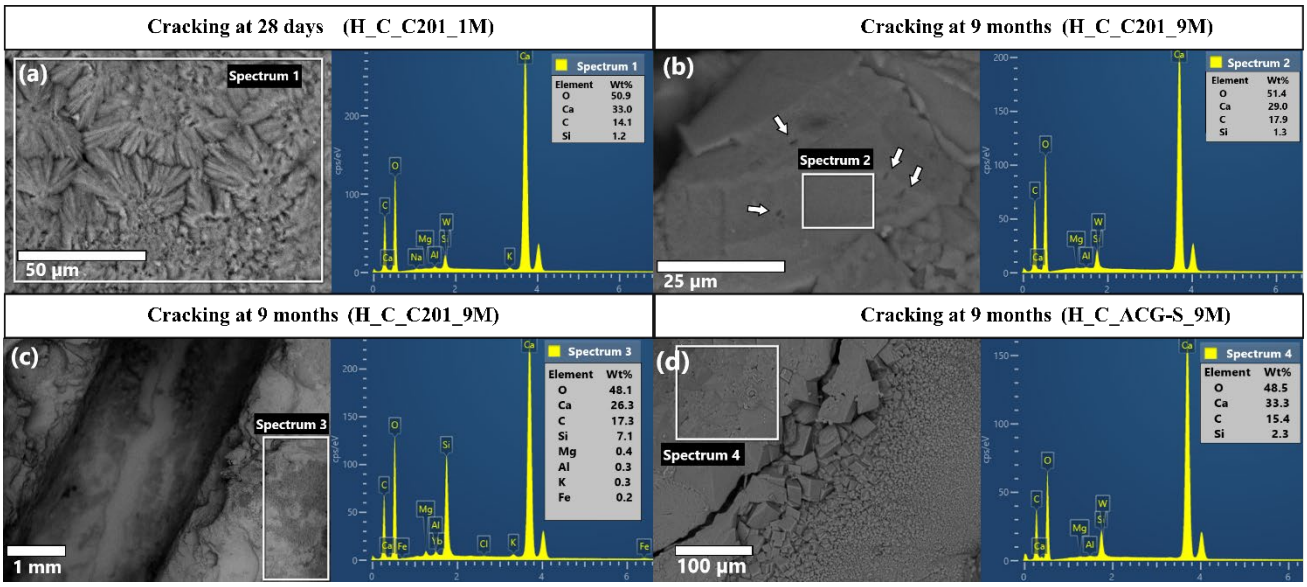

Fig. 13. SEM image and EDX analysis of self-healing products of H_C_C201 specimens. **(a)** H_C_C201_1M at the crack area (***spectrum 1***), **(b)** H_C_C201_9M at the crack area (***spectrum 2***), **(c)** H_C_C201_9M at a reference point located in the cement mortar matrix (***spectrum 3***) and **(d)** H_C_ACG-S_9M at the crack area (***spectrum 4***). The white arrow indicates surface bacteria imprints.

Raman spectroscopy –Raman microscopy analyses were conducted in the AEA-containing specimen (i.e., H_C_C201) to prove that the chemical structure of the precipitates formed within the crack corresponds to calcium carbonate (**Fig. 14**). **Fig. 14** shows that the mean value results of the Raman spectra acquired in each of the three H_C_C201_9M specimens are nearly identical, presenting a major band at 1087 cm^{-1} and other bands with lower relative intensity at 159, 282, 714, and 1440 cm^{-1}. These five bands correspond to the Raman spectra of pure calcite [66-68]. Therefore, the crystallisation products were corroborated to be calcium carbonate crystals (i.e., calcite) likely generated by microbial activity.

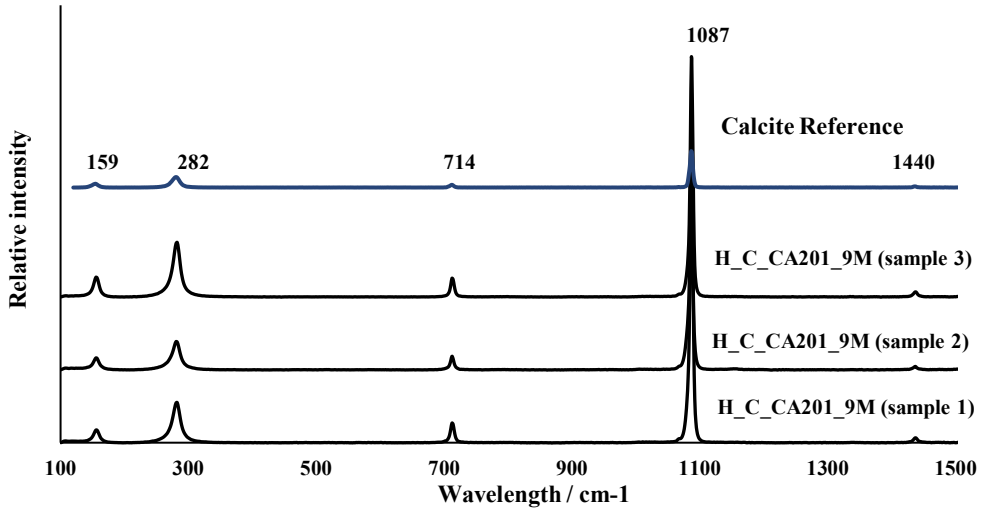

Fig. 14. Raman spectra showing the mean value for each of the three mortar specimens of H_C_C201_9M mortar mix.

3.6. *Economic evaluation*

A more economical and straightforward protection method for bacterial spores is crucial to reduce the current high production cost of BBSHCs. Therefore, it is important to evaluate if the use of AEAs represents a cost-effective alternative when compared to a successfully proven protection mechanism (i.e., ACGs). The laboratory process to produce ACG particles was used as the comparison for the economic evaluation. The cost of producing the bacterial spores was not considered within the cost analysis as it is assumed that the same amount of bacterial spores will be used for both alternatives. Moreover, capital investment costs were not considered as these depend on the production scale [69]. UK markets for energy, raw materials and laboratory technician salary were considered.

3.6.1. Production at laboratory scale

To calculate the operational costs associated with the production of 1 kg of ACGs based on laboratory scale setup, the materials needed (i.e., raw ACGs and polyvinyl acetate (PVA)), but also the energy (drying oven, vacuum pump and mixer) and labour requirements needed to embed the bacterial spores into these ACG particles are considered. The comparison of the operational costs for the two protection mechanisms is shown in **Table 4**.

Table 4: Comparison of the operational costs associated for the amount of ACGs or CX201 AEA needed to produce 1 m^3 of BBSHC (assumptions based on laboratory scale setup and previous studies [70]).

	ACGs	**C201 AEA**
Materials cost	1.34 €/kg	1.58 €/kg
Energy cost (0.17 €/kWh) [(1)]	0.249 €/kg	0.0 €/kg
Labour cost (19.80 €/h) [(2)]	1.32 €/kg	0.0 €/kg
Dose per 1 m^3 of BBSHC	45 kg [(3)]	6.16 L [(4)]
Total cost	130.95 €/m^3 of BBSHC	9.73 €/m^3 of BBSHC

[(1)] Energy cost in the UK for industrial consumers (www.gov.uk)
[(2)] Based on the average salary in the UK for a laboratory technician
[(3)] [70]
[(4)] C201 AEA dose of 0.017 L/kg cement

The amount of ACGs required for 1 m^3 of BBSHC (i.e., 45 kg/m^3) was assumed to be the same as when using a similar carrier (i.e., perlite) investigated in a previous study [70]. In contrast, only the operational cost associated with the required material (i.e., C201 AEA) is considered when AEAs are used to protect the bacterial spores. This protection mechanism does not involve the impregnation process that is required to embed the bacterial spores into the ACG particles. Consequently, bacterial spores are considered to be independently added during the initial concrete mixing process, and the cost of this activity is considered negligible.

4. Discussion

4.1. *Impacts of AEAs on spore viability and encapsulation*

Previous studies have shown that AEAs have no negative impact on cell viability when either vegetative cells or bacterial spores encapsulated in lightweight aggregates have been incorporated into BBSH cementitious composites [29, 38, 40]. However, the impact of AEA on bacterial spore viability had not been specifically investigated before. In this study, we demonstrated that the AEAs used in this study had no negative effects on spore viability or on the ability of *B. cohnii* spores to germinate (**Fig. 1**).

Hypothetically, it is assumed that the spores could be successfully trapped within the tiny air bubbles stabilised due to the use of these AEAs in mortar mixes. However, to demonstrate the presence of *B. cohnii* spores (size range of 0.8-1 µm [49]) inside these micro-air bubbles is not straightforward. Even using the most sophisticated µ-CT scans currently available, an almost impractical cement paste sample with a diameter size of 1 mm or less is required to obtain a µ-CT scan with a spatial distribution better than the size of the spores (~1 µm). In this study, a visual inspection using a compound microscope was conducted to validate if the bacterial spores could be successfully encapsulated inside the air micro-bubbles stabilised in agarose gel by the presence of AEAs. It was observed (**Fig. 2**) that a significant number of spores were trapped inside the tiny bubbles formed, regardless of the AEA type used. These results confirm that spores are not repelled from inside these micro-air bubbles, and that they are successfully encapsulated inside them.

4.2. *Comparison of healing in mortars without direct addition of bacterial spores.*

Visual observations (**Fig. 5** and **Fig. 6**) and area quantification (**Fig. 7**) showed no significant healing of the reference mortar mix (H_Reference) for either the Group II or Group III specimens. However, the average healing ratio (HR) percentage as a function of reduction in water-flow was observed higher for H_Reference Group II specimens compared to equivalent Group III specimens (**Fig. 10**). This was expected in the early-cracked Group II specimens and could be due to the higher availability of calcium hydroxide ($Ca(OH)_2$) reacting with atmospheric carbon dioxide (CO_2) to form calcium carbonates ($CaCO_3$) or from the higher amount of un-hydrated cement particles that were likely rehydrated (i.e., autogenous healing). However, since autogenous healing did not close the cracks in the H_Reference mortars, the crack healing observed in the other mortar mixes likely resulted from the direct addition of GM, microbiological activity or a combination of both.

As observed in **Fig. 7**, all mortar mixes cracked at 28 days (Group II) presented a significantly better healing performance when compared to equivalent mortar mixes of Group III cracked at a later age (9 months). The direct addition of calcium nitrate (i.e., 5% by cement mass) and the use of Portland-limestone cement likely resulted in increased availability of calcium hydroxides. On the other hand, the use of tap water and open containers (atmospheric CO_2) during the curing process likely decreased the available calcium hydroxide. Tap water was selected over lime-saturated water to reproduce more realistic conditions, and this could likely have resulted in potentially higher leaching of calcium-rich healing products from the cement matrix to the curing water before crack formation. Based on the considerable availability of calcium hydroxides and an inorganic carbon source, the following hypotheses are suggested to explain the significant formation of precipitates within the cracks of these mortar specimens (Group II):

The precipitation of calcium hydroxide crystals in the cracks occurs in the liquid phase, where the cracks are completely or partially filled with water during the formation of these crystals. Ca^{2+} ions are transported (by diffusion) from the supersaturated pore solution inside the mortar matrix to the water present in the cracks. This leaching likely allows the concentration of Ca^{2+} ions to build up within the cracks and reach the supersaturation conditions needed for their precipitation [71, 72]. Then, the calcium hydroxide precipitated is transformed into $CaCO_3$ due to the dissolution of atmospheric CO_2 into the water within the crack. Moreover,

due to the differences in the physical properties of these two minerals, the volume of calcium hydroxide precipitates would increase by 10% when it transforms into $CaCO_3$ [73]. Other factors could have influenced the migration of calcium hydroxide from inside the mortar matrix to the cracks. In this context, it is known that certain organic compounds can increase the solubility of calcium hydroxide considerably [71]. In this study, the higher availability of yeast extract at early ages could have increased the migration rate of Ca^{2+} ions. Another possible explanation for this enhanced healing at early ages could be the combination of yeast extract, calcium hydroxide and environmental bacteria. Environmental bacteria could have contributed to the healing of the cracks, as tap water and non-sterile conditions were used to reproduce realistic conditions during curing and healing. A likely scenario for this would be the metabolic breakdown of the yeast extract leading to CO_2 release and thus an increased concentration of carbonate ions to form precipitates with the Ca^{2+} ions provided by calcium hydroxide. In contrast, when a calcium precursor was directly added and cracking occurred at a later age (9 months; Group III specimens), it appears that fewer Ca^{2+} ions were available to be leached and reprecipitated within the cracks. This decrease in Ca^{2+} ions was likely due to the leaching of calcium-rich healing products from the mortar matrix into the curing tap water over a more extended curing period or due to carbonation resulting from the dissolution of atmospheric CO_2 into the curing water. Similar observations were reported by Tan et al. [19] when investigating the self-healing performance of carbonated mortar specimens.

In this context, for 28-days cracked control mortar specimens (i.e., H_C_Ø_1M), the average HR was equal to 79.4%, while for specimens cracked at 9 months of age, the average HR was equal to 11.7%. These results show that H_C_Ø specimens cracked at an early age have significantly improved healing compared to the later cracked specimens. Furthermore, it was observed that in the H_C_ Ø_1M specimens, the degree of healing was similar to the degree of healing observed when GM was included in the mortar in an encapsulated form in H_R+ACG-GM_ACG-S mortars (discussed below). When calcium precursors are directly added, it has been reported that this can increase the quantities of calcium hydroxide, and consequently, the calcium ions available at early ages for autonomous self-healing [19].

Furthermore, as shown in **Fig. 8**, when the specimens were cracked after 28 days of curing and allowed to self-heal for 56 days, a significant percentage of all the measured crack widths (i.e., 55.6%) showed a HR of 100%, while 26.4% of the crack widths showed a HR below 10%. In contrast, when the specimens were cracked after 9 months and left to self-heal for 56 days, the percentages were inversed, where the crack widths achieving a 100% HR represented only 25.9% of all the measured cracks, while the crack widths experiencing a HR below 10% comprised 50.7%. Thus, the crack width results are in accordance with the crack area reduction observed in **Fig. 5** and **6**.

Fig. 7 shows the HRs for H_R+ACG-GM_ACG-S specimens where the bacterial spores and growth media were independently encapsulated. Specimens of this mortar mix presented only a slightly higher average HR when cracked at 28 days (83.2%) compared to 9 months (75.5%). In this case, the slightly higher HR observed when cracked at an early age likely resulted from the rehydration of a higher number of un-hydrated cement particles or the availability of additional calcium hydroxides generated by the hydration of cement within the cement matrix, but could also be related to the number of ACG particles broken by the crack. When cracked at 9 months, H_R+ACG-GM_ACG-S specimens presented the best SH performance of all the mortar mixes investigated in this study. As this was the only mortar mix where the GM was encapsulated and not directly added during the initial mixing, it is likely that the significantly higher amount of calcium and yeast extract available to the bacteria when the crack was formed at a later age contributed to this efficiency. Moreover, the average HR observed as a function of reduction in water-flow for the H_R+ACG-GM_ACG-S mortar mix was very similar (72.5%), thus demonstrating efficient healing (**Fig. 10)**.

When the self-healing performance of cementitious composites is investigated, a key aspect to consider is the cracking age [42, 52], especially when GM is added directly with the mixing water. In this regard, the healing capacity results observed in this study suggest that when the mortar specimens are cracked at an early age (i.e., 28 days), direct inclusion of calcium precursors and nutrients are likely sufficient to achieve crack healing. However, when mortar specimens are cracked at a later age (i.e., 9 months), this is no longer the case, and satisfactory healing efficiencies depend completely on the addition and adequate protection of bacterial spores, calcium precursors and nutrients. Thus, the results in this study support the argument that the availability of calcium hydroxides at later ages needs to be considered in practice [19, 42, 48].

4.3. *Comparison of self-healing in mortars containing AEAs*

In this study, the efficiency of the AEAs to encapsulate bacterial spores was evaluated by comparing the healing results of the four mortar mixes where the bacterial spores and GM were directly added during the initial mixing process (i.e., H_C_SD, H_C_C201, H_C_B119 and H_C_B130) (**Fig. 7**). Similar to what was observed for the other mortar mixes mentioned in the previous subsection, specimens cracked at an early age (28 days) presented higher HRs principally due to the likely greater availability of inorganic carbon and calcium hydroxide resulting from the direct addition of GM. Nevertheless, as explained below, the observations from the later-aged cracked specimens allowed a better comparison of the healing efficiencies among these four mortar mixes.

When comparing the H_C_SD_9M mix with an equivalent mix without bacterial spores (i.e., H_C_Ø_9M), the healing efficiency observed was 25.8% and 11.7%, respectively. This two-fold healing efficiency value observed for the H_C_SD_9M mix suggests that some of the original bacterial spores added during the initial mixing could survive the initial harsh conditions and reactivate once the crack was formed after a curing period of 9 months. As shown in **Fig. 3** and reported by other researchers [58], the direct addition of yeast extract in mortar mixes results in significant air content increases. This effect could likely be attributed to the amphiphilic compounds found in yeast extract. [74]. Consequently, the additional air voids produced by adding yeast extract could have likely protected some of the directly added spores, similar to the mechanism observed with AEAs.

For the 9-months-old specimens results shown in **Fig. 7**, the H_C_C201 mix presented the best healing performance compared to the other three AEA-containing mixes. In this regard, the H_C_C201 presented an average HR of 54.4% compared to 25.8%, 9.2% and 37.1% of H_C_SD, H_C_B119 and H_C_B130 mixes, respectively. Moreover, as is shown in **Fig. 10**, a similar trend in terms of healing performance was observed in the recovery of the water-flow resisting properties, where the H_C_C201 mix also resulted in the highest average HR (84.8%) of all these mortar mixes and presented the least variability among specimens. Contrary to what was expected, the worst performance was not observed for the mix without AEA addition (i.e., H_C_SD) but for the H_C_B119 mix containing an anionic AEA. The size distribution and total area of the micro-bubbles were analysed in a representative specimen of each of the AEA-containing mortar mixes and the results are shown in **Fig. 15**.

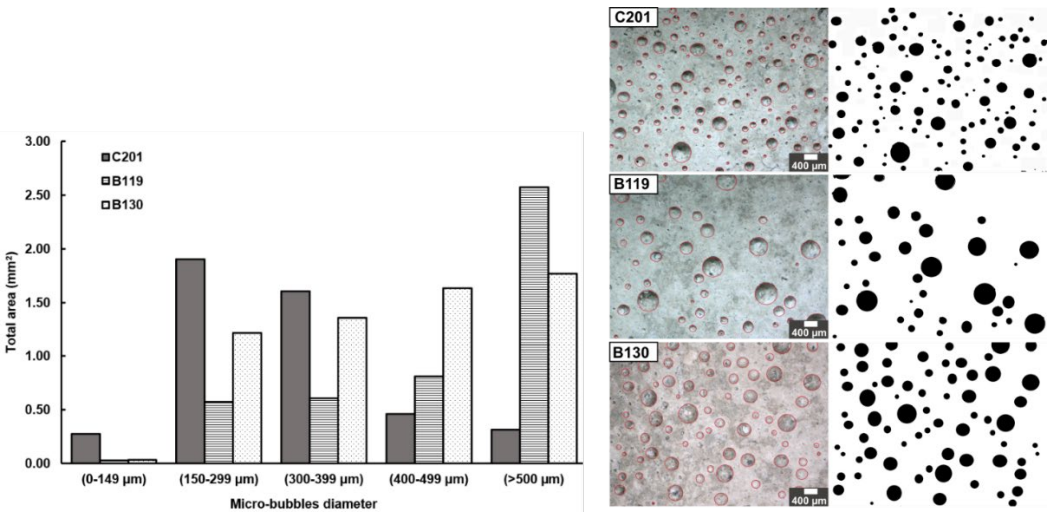

Fig. 15. Micro-bubbles total area (mm^2) *(left)* and size distribution *(right)* were obtained from a representative mortar specimen of the following mixes: H_C_C201_9M, H_C_B119_9M and H_C_B130_9M. A digital microscope (Keyence VHX-6000, Japan) was used at a 50x magnification.

From the size distribution of the micro-bubbles (Fig. 15), it was observed that the percentage of bubbles with a diameter of less than 0.3 mm was 47.8%, 13.2% and 20.8% for C201, B119 and B130 AEAs, respectively. Moreover, the total area for all the micro-bubbles formed was similar for C201 and B119 specimens (i.e., 4.5 mm^2), while the B130 specimen presented a higher total area (6.0 mm^2). It is known that the air-void system and the stability of the micro-bubbles formed strictly depends on the type of surfactants present in the AEAs

[75]. Fatty alcohol types AEAs (such as C201) are known to produce smaller micro-bubbles, while synthetic and resin types (such as B119 and B130) form coarser and mid-sized micro-bubbles, respectively [74]. In this regard, the formation of a greater number of smaller micro-bubbles (i.e., <0.3 mm) is likely to have had a greater influence on the healing process than the total area of micro-bubbles formed. In this context, the higher amount and more homogeneous distribution of these smaller micro-bubbles (containing bacterial spores) could have resulted in more micro-bubbles hit by the crack and thus increased the number of bacterial spores available to start the healing process. Overall, it is hypothesised that the differences observed in the healing performance between the three AEA-containing mortar mixes could likely result from micro-bubbles size distribution but also the interactions of each type of surfactant with the spores, GM and the cement matrix. Further research will be needed to fully elucidate the interactions between these components.

The healing performance observed among the AEAs mixes was unlikely to have been influenced by the average crack width, as this was very similar for all samples, in a range between 0.43 and 0.59 mm for Group II and between 0.48 and 0.51 mm for Group III (**Table 3**). Further comparison was made of the H_C_C201 healing performance when contrasted to the mortar mix where the bacterial spores were encapsulated using ACG (i.e., (H_C_ACG-S). When analysing the healing results obtained from the crack binarization images of the 9-months-old specimens (**Fig. 7**), the healing performance of the H_C_C201 mix was ~45% higher than that observed for the H_C_ACG-S mix. However, when comparing the recovery of the water-flow resisting properties, the results observed among these two mixes were very similar with 84.8% and 84.0%, respectively (**Fig. 10**). Moreover, when the H_C_C201 mix was contrasted to the H_R+ACG-GM_ACG-S mix, where the bacterial spores and GM were independently encapsulated, the latter presented a significantly higher average HR when cracked at 9 months of 54.4% and 75.5%, respectively (**Fig. 7**). However, when comparing the average HR obtained with the water-flow tests, the HR of the H_C_C201 was better (84.8%) than the observed for the H_R+ACG-GM_ACG-S mix (72.5%) (**Fig. 10**). Overall, despite visual differences in the crack closure performance, the similar water tightness results likely show that the cracks were similarly sealed.

Regarding the economic benefits of using AEAs to protect bacterial spores, the cost of spore protection is 13 times lower than when using ACGs to achieve similar healing efficiencies. Moreover, the overall process is significantly more straightforward as there is no need for a previous step to embed these spores. However, the simple cost analysis conducted is based on the operational costs of a laboratory-scale setup and where capital investment costs were not considered. Therefore, it is expected that the process for producing bacteria-laden ACGs will be optimised to achieve an industrially feasible process, and this could potentially reduce the cost difference between these two protection methods.

To summarise, these results suggest the capability of some AEAs to successfully protect directly added spores in a similar way as other proven encapsulation methods (i.e., ACGs), and this opens the doors to the development of bespoke AEAs that could result in a more straightforward and economical encapsulation method for bacterial spores in SH cementitious composites.

5 Conclusions

The purpose of this study was to explore the feasibility of using air-entraining admixtures (AEAs), commonly used in concrete industry, as a protection method for bacterial spores when these spores are directly added to BBSH cementitious materials. The following major conclusions can be drawn:

1. AEAs have no negative effects on spore viability or on the ability of *B. cohnii* spores to germinate. Consequently, they are an effective means of encapsulating spores whilst distributing them homogeneously throughout the mortar.
2. The encapsulation of spores in air voids leads to effective self-healing. In the case of C201 AEA healing was approximately 60% better than other proven protection methods for cracks formed at 28 days and approximately 45% better for those formed at 9 months. Moreover, water penetration resistance was increased by 18% or presented very similar values for early or later-formed cracks, respectively
3. The variations in performance between different AEAs is most likely due to differences in the size distribution of the micro bubbles that are formed; with smaller bubble formation leading to improved performance due to potentially improved distribution of spores.
4. Better self-healing performance is observed when equivalent mortar specimens are cracked at 28 days than at later ages (9 months). This is most likely due to the Ca^{2+} ions and carbon source becoming trapped in a form that is not readily available to added or environmental bacteria.

5. The cost of using AEAs to protect directly added bacterial spores in BBSHCs is about 13 times lower than when these spores are embedded into ACG particles to achieve similar healing efficiencies.

Encapsulation of bacterial spores *via* AEAs has significant benefits over other encapsulation methods, as it represents a more economical and straightforward approach. This study shows that not all AEAs have the same performance and opens the doors to the development of bespoke AEAs. Moreover, it was demonstrated the survival of *B. cohnii* spores in mortars when cracks appear either at an early age (28 days) or a later age (9 months). Further research is needed to optimise the use of these AEAs by improving the mechanical properties of the cementitious material while protecting the highest possible number of bacterial spores. Overall, the results of this study are very promising for developing BBSHCs able to self-repair microcracks produced by early age shrinkage and repetitive or excessive loading at later ages.

Data availability

All data created during this research are openly available from the University of Bath Research Data Archive at https://doi.org/10.15125/BATH-01087 [dataset] [76].

Authors' contributions

IJR: Conceptualisation, Formal analysis, Investigation, Methodology, Visualisation, Writing - original draft. **BR:** Investigation, Writing – review & editing. **CHB:** Investigation, Writing – review & editing. **AH:** Funding acquisition, Supervision, Writing – review & editing. **SG:** Conceptualisation, Funding acquisition, Methodology, Supervision, Writing – review & editing. **KP**: Conceptualisation, Funding acquisition, Methodology, Project administration, Supervision, Writing – original draft.

Declaration of competing interest

The authors declare that they have no known competing financial interests or personal relationships that could have appeared to influence the work reported in this paper.

Acknowledgements

This work was supported by the EPSRC through the Resilient Materials for Life (RM4L) (EP/P02081X/1) and the Engineering Microbial-Induced Carbonate Precipitation *via* Meso-Scale Simulations (eMICP) (EP/S013997/1) projects. The authors gratefully acknowledge the technical staff in the Department of Architecture and Civil Engineering, the Department of Biology and Biochemistry and the Material and Chemical Characterisation Facility (MC^2) at the University of Bath (https://doi.org/10.15125/mx6j-3r54) for their key support. The authors further thank Paul J. Griffin (Cemex Admixtures UK) and Ian Ellis (BASF Construction Chemicals (UK) Ltd.) for providing the AEAs.

REFERENCES

[1] P. Mehta, Paulo, Monteiro, Paulo JM, Concrete: microstructure, properties, and materials, 0071462899, 2006.
[2] X. Xi and S. Yang, Time to surface cracking and crack width of reinforced concrete structures under corrosion of multiple rebars, *Construction and Building Materials,* vol. 155, pp. 114-125, 2017.
[3] T.-T. Le, V.-H. Nguyen, and M. V. Le, Development of deep learning model for the recognition of cracks on concrete surfaces, *Applied Computational Intelligence and Soft Computing,* vol. 2021, 2021.
[4] K. Van Tittelboom and N. De Belie, Self-healing in cementitious materials—A review, *Materials,* vol. 6, no. 6, pp. 2182-2217, 2013.
[5] I. Justo-Reinoso, A. Heath, S. Gebhard, and K. Paine, Aerobic non-ureolytic bacteria-based self-healing cementitious composites: A comprehensive review, *Journal of Building Engineering,* vol. 42, no. 102834, pp. 1-25, 2021/06/05/ 2021, doi: https://doi.org/10.1016/j.jobe.2021.102834.
[6] A. Danish, M. A. Mosaberpanah, and M. U. Salim, Past and present techniques of self-healing in cementitious materials: A critical review on efficiency of implemented treatments, *Journal of Materials Research and Technology,* 2020.
[7] N. De Belie, B. Van Belleghem, and P. Van den Heede, Durability and sustainability of self-healing concrete, in *Int. Conference on" Cement-based materials tailored for a sustainable future"(CBMT)*, 2021, pp. 55-67.

[8] R. Mors and H. M. Jonkers, Bacteria-based self-healing concrete: evaluation of full scale demonstrator projects, *RILEM Technical Letters,* vol. 4, pp. 138-144, 2020.
[9] G. Perez, E. Erkizia, J. Gaitero, I. Kaltzakorta, I. Jiménez, and A. Guerrero, Synthesis and characterization of epoxy encapsulating silica microcapsules and amine functionalized silica nanoparticles for development of an innovative self-healing concrete, *Materials Chemistry and Physics,* vol. 165, pp. 39-48, 2015.
[10] C. Litina and A. Al-Tabbaa, First generation microcapsule-based self-healing cementitious construction repair materials, *Construction and Building Materials,* vol. 255, p. 119389, 2020.
[11] W. Mao, C. Litina, and A. Al-Tabbaa, Development and Application of Novel Sodium Silicate Microcapsule-Based Self-Healing Oil Well Cement, *Materials,* vol. 13, no. 2, p. 456, 2020.
[12] S. Farhadi and S. Ziadloo, Self-Healing Microbial Concrete-A Review, in *Materials Science Forum*, 2020, vol. 990: Trans Tech Publ, pp. 8-12.
[13] H. Kim, H. Son, J. Seo, and H.-K. Lee, Recent advances in microbial viability and self-healing performance in bacterial-based cementitious materials: A review, *Construction and Building Materials,* vol. 274, p. 122094, 2021.
[14] T. D. Hoffmann, B. J. Reeksting, and S. Gebhard, Bacteria-induced mineral precipitation: a mechanistic review, *Microbiology,* vol. 167, no. 4, p. 001049, 2021.
[15] H. M. Jonkers and E. Schlangen, Crack repair by concrete-immobilized bacteria, in *Proceedings of the first international conference on self healing materials*, 2007, vol. 18, p. 20.
[16] E. Tziviloglou, V. Wiktor, H. Jonkers, and E. Schlangen, Bacteria-based self-healing concrete to increase liquid tightness of cracks, *Construction and Building Materials,* vol. 122, pp. 118-125, 2016.
[17] S. Han, I. Jang, E. K. Choi, W. Park, C. Yi, and N. Chung, Bacterial Self-Healing Performance of Coated Expanded Clay in Concrete, *Journal of Environmental Engineering,* vol. 146, no. 7, p. 04020072, 2020, doi: doi:10.1061/(ASCE)EE.1943-7870.0001713.
[18] M. Rauf, W. Khaliq, R. A. Khushnood, and I. Ahmed, Comparative performance of different bacteria immobilized in natural fibers for self-healing in concrete, *Construction and Building Materials,* vol. 258, p. 119578, 2020.
[19] L. Tan, B. Reeksting, V. Ferrandiz-Mas, A. Heath, S. Gebhard, and K. Paine, Effect of carbonation on bacteria-based self-healing of cementitious composites, *Construction and Building Materials,* vol. 257, no. 119501, pp. 1-13, 2020.
[20] O. Hamza, M. Esaker, D. Elliott, and A. Souid, The effect of soil incubation on bio self-healing of cementitious mortar, *Materials Today Communications,* vol. 24, p. 100988, 2020.
[21] M. Zamani, S. Nikafshar, A. Mousa, and A. Behnia, Bacteria encapsulation using synthesized polyurea for self-healing of cement paste, *Construction and Building Materials,* vol. 249, p. 118556, 2020.
[22] R. Mors and H. Jonkers, Effect on concrete surface water absorption upon addition of lactate derived agent, *Coatings,* vol. 7, no. 4, p. 51, 2017.
[23] X. Zhu *et al.*, Viability determination of Bacillus sphaericus after encapsulation in hydrogel for self-healing concrete via microcalorimetry and in situ oxygen concentration measurements, *Cement and Concrete Composites,* vol. 119, p. 104006, 2021.
[24] M. Gao *et al.*, Immobilized bacteria with pH-response hydrogel for self-healing of concrete, *Journal of environmental management,* vol. 261, p. 110225, 2020.
[25] N. B. Filipe Bravo Silva, Nele de Belie and Willy Verstraete, Industrial Application of Biological Self-healing Concrete: Challenges and Economical Feasibility, *Journal of Commercial Biotechnology,* vol. 21, no. 1, pp. 31-38, January 2015 2015, doi: doi.org/10.5912/jcb662.
[26] P. Mehta and P. J. Monteiro, *Concrete: Microstructure, Properties, and Materials*, Third Edition ed. New York: Mc Graw Hill, 2006, p. 659.
[27] L. Du and K. J. Folliard, Mechanisms of air entrainment in concrete, *Cement and concrete research,* vol. 35, no. 8, pp. 1463-1471, 2005.
[28] B. Łaźniewska-Piekarczyk, The influence of selected new generation admixtures on the workability, air-voids parameters and frost-resistance of self compacting concrete, *Construction and Building Materials,* vol. 31, pp. 310-319, 2012.
[29] Z. B. Bundur, A. Amiri, Y. C. Ersan, N. Boon, and N. De Belie, Impact of air entraining admixtures on biogenic calcium carbonate precipitation and bacterial viability, *Cement and Concrete Research,* vol. 98, pp. 44-49, 2017.
[30] J. Xu *et al.*, Influence of surfactants on chloride binding in cement paste, *Construction and Building Materials,* vol. 125, pp. 369-374, 2016.
[31] Q. Liu, Z. Chen, and Y. Yang, Study of the Air-Entraining Behavior Based on the Interactions between Cement Particles and Selected Cationic, Anionic and Nonionic Surfactants, *Materials,* vol. 13, no. 16, p. 3514, 2020.
[32] V. H. Dodson, *Concrete admixtures*. Springer Science & Business Media, 2013.
[33] F. Lea, The Chemistry of Cement and Concrete. 3rd edn, E, *Arnold, London,* 1970.
[34] K.-S. Chia and M.-H. Zhang, Workability of air-entrained lightweight concrete from rheology perspective, *Magazine of Concrete Research,* vol. 59, no. 5, pp. 367-375, 2007, doi: 10.1680/macr.2007.59.5.367.
[35] M. Wilson and S. Kosmatka, Design and control of concrete mixtures, *Portland Cement Association: USA,* 2011.
[36] Y. Ç. Erşan, F. B. Da Silva, N. Boon, W. Verstraete, and N. De Belie, Screening of bacteria and concrete compatible protection materials, *Construction and Building Materials,* vol. 88, pp. 196-203, 2015, doi: 10.1016/j.conbuildmat.2015.04.027.
[37] J. Luo *et al.*, Interactions of fungi with concrete: Significant importance for bio-based self-healing concrete, *Construction and building materials,* vol. 164, pp. 275-285, 2018.
[38] C. Stuckrath, R. Serpell, L. M. Valenzuela, and M. Lopez, Quantification of chemical and biological calcium carbonate precipitation: performance of self-healing in reinforced mortar containing chemical admixtures, *Cement and Concrete Composites,* vol. 50, pp. 10-15, 2014.

[39] N. Parastegari, D. Mostofinejad, and D. Poursina, Use of bacteria to improve electrical resistivity and chloride penetration of air-entrained concrete, *Construction and Building Materials,* vol. 210, pp. 588-595, 2019.
[40] B. Chen *et al.*, Crack sealing evaluation of self-healing mortar with Sporosarcina pasteurii: Influence of bacterial concentration and air-entraining agent, *Process Biochemistry,* vol. 107, pp. 100-111, 2021.
[41] B. J. Reeksting, T. D. Hoffmann, L. Tan, K. Paine, and S. Gebhard, In-depth profiling of calcite precipitation by environmental bacteria reveals fundamental mechanistic differences with relevance to application, *Applied and Environmental Microbiology,* vol. 86, no. 7, pp. 1-16, 2020.
[42] E. Rossi, C. M. Vermeer, R. Mors, R. Kleerebezem, O. Copuroglu, and H. M. Jonkers, On the applicability of a precursor derived from organic waste streams for bacteria-based self-healing concrete, *Frontiers in Built Environment,* vol. 7, p. 2, 2021.
[43] Y. Ç. Erşan, E. Hernandez-Sanabria, N. Boon, and N. De Belie, Enhanced crack closure performance of microbial mortar through nitrate reduction, *Cement and concrete composites,* vol. 70, pp. 159-170, 2016.
[44] Y. Ç. Erşan, E. Gruyaert, G. Louis, C. Lors, N. De Belie, and N. Boon, Self-protected nitrate reducing culture for intrinsic repair of concrete cracks, *Frontiers in microbiology,* vol. 6, p. 1228, 2015.
[45] M. Luo and C. X. Qian, Performance of two bacteria-based additives used for self-healing concrete, *Journal of Materials in Civil Engineering,* vol. 28, no. 12, p. 04016151, 2016.
[46] T. Zheng and C. Qian, Self-healing of later-age cracks in cement-based materials by encapsulation-based bacteria, *Journal of Materials in Civil Engineering,* vol. 32, no. 11, p. 04020341, 2020.
[47] V. Wiktor and H. M. Jonkers, Quantification of crack-healing in novel bacteria-based self-healing concrete, *Cement and Concrete Composites,* vol. 33, no. 7, pp. 763-770, 2011.
[48] L. Skevi, B. Reeksting, S. Gebhard, and K. Paine, Bacteria Based Self-healing of Later-Age Cracks in Concrete, Cham, 2021: Springer International Publishing, in International RILEM Conference on Early-Age and Long-Term Cracking in RC Structures, pp. 367-376.
[49] H. M. Jonkers, A. Thijssen, G. Muyzer, O. Copuroglu, and E. Schlangen, Application of bacteria as self-healing agent for the development of sustainable concrete, *Ecological engineering,* vol. 36, no. 2, pp. 230-235, 2010.
[50] H. Zhang, *Building materials in civil engineering*. Elsevier, 2011.
[51] P. Lawrence, E. Ringot, and B. Husson, About the measurement of the air content in mortar, *Materials and structures,* vol. 32, no. 8, pp. 618-621, 1999.
[52] L. Ferrara *et al.*, Experimental characterization of the self-healing capacity of cement based materials and its effects on the material performance: a state of the art report by COST Action SARCOS WG2, *Construction and building materials,* vol. 167, pp. 115-142, 2018.
[53] M. Roig-Flores, F. Pirritano, P. Serna, and L. Ferrara, Effect of crystalline admixtures on the self-healing capability of early-age concrete studied by means of permeability and crack closing tests, *Construction and Building Materials,* vol. 114, pp. 447-457, 2016.
[54] M. D. Abràmoff, P. J. Magalhães, and S. J. Ram, Image processing with ImageJ, *Biophotonics International,* vol. 11, no. 7, pp. 36-42, 2004.
[55] M. Stefanidou, E. Tsampali, G. Karagiannis, S. Amanatiadis, A. Ioakim, and S. Kassavetis, Techniques for recording self-healing efficiency and characterizing the healing products in cementitious materials, *Material Design & Processing Communications,* 2020.
[56] M. Luo, C.-x. Qian, and R.-y. Li, Factors affecting crack repairing capacity of bacteria-based self-healing concrete, *Construction and building materials,* vol. 87, pp. 1-7, 2015.
[57] *RILEM Test Method 11.4: Measurement of water absorption under low pressure*, RILEM, Paris, France., 1987.
[58] X. Chen, J. Yuan, and M. Alazhari, Effect of microbiological growth components for bacteria-based self-healing on the properties of cement mortar, *Materials,* vol. 12, no. 8, p. 1303, 2019.
[59] E. Yurdakul, P. C. Taylor, H. Ceylan, and F. Bektas, Effect of water-to-binder ratio, air content, and type of cementitious materials on fresh and hardened properties of binary and ternary blended concrete, *Journal of materials in civil engineering,* vol. 26, no. 6, p. 04014002, 2014.
[60] M. Soutsos, *Concrete durability: A practical guide to the design of durable concrete structures.* London: Thomas telford, 2010.
[61] S. Bhaskar, K. M. A. Hossain, M. Lachemi, G. Wolfaardt, and M. O. Kroukamp, Effect of self-healing on strength and durability of zeolite-immobilized bacterial cementitious mortar composites, *Cement and Concrete Composites,* vol. 82, pp. 23-33, 2017.
[62] K. Scrivener, R. Snellings, and B. Lothenbach, *A Practical Guide to Microstructural Analysis of Cementitious Materials*. Crc Press, 2016.
[63] Z. Yan-Rong *et al.*, Influence of triethanolamine on the hydration product of portlandite in cement paste and the mechanism, *Cement and Concrete Research,* vol. 87, pp. 64-76, 2016.
[64] A. Elyamani, M. S. El-Rashidy, M. Abdel-Hafez, and H. Gad El-Rab, A contribution to the conservation of 20th century architectural heritage in Khedival Cairo, *International Journal of Conservation Science,* vol. 9, no. 1, 2018.
[65] F. Matalkah, P. Soroushian, A. Balchandra, and A. Peyvandi, Characterization of alkali-activated nonwood biomass ash–based geopolymer concrete, *Journal of Materials in Civil Engineering,* vol. 29, no. 4, p. 04016270, 2017.
[66] A. Leemann, Raman microscopy of alkali-silica reaction (ASR) products formed in concrete, *Cement and Concrete Research,* vol. 102, pp. 41-47, 2017.
[67] J. Sun, Z. Wu, H. Cheng, Z. Zhang, and R. L. Frost, A Raman spectroscopic comparison of calcite and dolomite, *Spectrochimica Acta Part A: Molecular and Biomolecular Spectroscopy,* vol. 117, pp. 158-162, 2014.

[68] L. Black, C. Breen, J. Yarwood, K. Garbev, P. Stemmermann, and B. Gasharova, Structural features of C–S–H (I) and its carbonation in air—a Raman spectroscopic study. Part II: carbonated phases, *Journal of the American Ceramic Society,* vol. 90, no. 3, pp. 908-917, 2007.
[69] F. B. Da Silva, N. De Belie, N. Boon, and W. Verstraete, Production of non-axenic ureolytic spores for self-healing concrete applications, *Construction and Building Materials,* vol. 93, pp. 1034-1041, 2015.
[70] K. Paine, M. Alazhari, T. Sharma, R. Cooper, and A. Heath, Design and performance of bacteria-based self-healing concrete, in *The 9th International Concrete Conference 2016: Environment, Efficiency and Economic Challenges for Concrete*, 2016, pp. 545-554.
[71] H. Bache, G. Idorn, P. Nepper-Christensen, and J. Nielsen, Morphology of calcium hydroxide in cement paste, *HRB Special Report,* vol. 90, pp. 154-174, 1966.
[72] C. Edvardsen, Water permeability and autogenous healing of cracks in concrete, in *Innovation in Concrete Structures: Design and Construction*: Thomas Telford Publishing, 1999, pp. 473-487.
[73] H. Huang, G. Ye, and D. Damidot, Characterization and quantification of self-healing behaviors of microcracks due to further hydration in cement paste, *Cement and Concrete Research,* vol. 52, pp. 71-81, 2013.
[74] Y. Şahin, Y. Akkaya, F. Boylu, and M. Taşdemir, Characterization of air entraining admixtures in concrete using surface tension measurements, *Cement and Concrete Composites,* vol. 82, pp. 95-104, 2017.
[75] H. A. Shah, Q. Yuan, and S. Zuo, Air entrainment in fresh concrete and its effects on hardened concrete-a review, *Construction and Building Materials,* vol. 274, p. 121835, 2021.
[76] I. Justo-Reinoso, Reeksting, B., Hamley-Bennett, C., Heath, A., Gebhard, S., Paine, K. *In press. Dataset for "Air-entraining admixtures as a protection mechanism for bacterial spores in self-healing cementitious composites: Healing evaluation of early and later-age cracks"*, Bath: University of Bath Research Data Archive, 28 October 2021, doi: http://doi.org/10.15125/BATH-01087.